

1 **MULTI YEAR AEROSOL CHARACTERIZATION IN THE TROPICAL**
2 **ANDES AND IN ADJACENT AMAZONIA USING AERONET**
3 **MEASUREMENTS**

4
5 Daniel Pérez-Ramírez^{a,b}, Marcos Andrade-Flores^{c,d}, Thomas F. Eck^{e,f}, Ariel F.
6 Stein^g, Norman T. O'Neill^h, Hassan Lyamani^{a,b}, Santiago Gassó^{i,j}, David N.
7 Whiteman^k, Igor Veselovskii^{l,m}, Fernando Velarde^c and Alados-Arboledas, L.^{a,b}
8

9 ^aApplied Physics Department, University of Granada, 18071, Granada, Spain

10 ^bAndalusian Institute for Earth System Research (IISTA), Av.Mediterráneo s/n, 18006, Granada,
11 Spain

12 ^cLaboratory for Atmospheric Physics, Universidad Mayor de San Andrés, La Paz, Bolivia.

13 ^dDepartment of Atmospheric and Oceanic Sciences, University of Maryland, College Park,
14 Maryland, United States

15 ^eGoddard Earth Sciences Technology and Research, University Space Research Association
16 (GESTAR/USRA), 21040, Columbia, Maryland, United States

17 ^fBiospheric Sciences Laboratory, NASA Goddard Space Flight Center, 20771, Greenbelt,
18 Maryland, United States.

19 ^gNOAA Air Resources Laboratory, 5830 University Research Court, 20740, College Park,
20 Maryland, United States

21 ^hCentre d'Applications et de Recherches en Télédétection, Université de Sherbrooke,
22 Sherbrooke, Canada

23 ⁱMorgan State University, Maryland, United States

24 ^jClimate and Radiation Laboratory, NASA Goddard Space Flight Center, 20771, Greenbelt,
25 Maryland, United States.

26 ^kMesoscale Atmospheric Processes Laboratory, NASA Goddard Space Flight Center, 20771,
27 Greenbelt, Maryland, United States.

28 ^lJoint Center for Earth Systems Technology, University of Maryland Baltimore County,
29 Baltimore, Maryland, United States.

30 ^mPhysics Instrumentation Center of General Physics Institute, Troitsk, Moscow, Russia

31
32
33
34
35 Correspondence to: Daniel Perez-Ramirez; E-mail: dperez@ugr.es;

36 **ABSTRACT**

37 This work focuses on the analysis of columnar aerosol properties in the complex
38 geophysical tropical region of South America within 10-20° South and 50-70° West. The region
39 is quite varied and encompasses a significant part of Amazonia (lowlands) as well as high
40 mountains in the Andes (highlands, ~4000 m a.s.l.). Several AERONET stations were included to
41 study the aerosol optical characteristics of the lowlands (Rio Branco, Ji Parana and Cuiaba in
42 Brazil and Santa Cruz in Bolivia) and the highlands (La Paz, Bolivia) during the 2000-2014
43 period. Biomass-burning is by far the most important source of aerosol in the lowlands,
44 particularly during the dry season (August-October). Multi-annual variability was investigated
45 and showed very strong burning activity in 2005, 2006, 2007 and 2010. This resulted in smoke
46 characterized by correspondingly strong, above-average AODs (aerosol optical depths) and
47 homogeneous single scattering albedo (SSA) across all the stations (~0.93). For other years,
48 however, SSA differences arise between the northern stations (Rio Branco and Ji Parana) with
49 SSAs of ~0.95 and the southern stations (Cuiaba and Santa Cruz) with lower SSAs of ~0.85.
50 Such differences are explained by the different types of vegetation burned in the two different
51 regions. In the highlands, however, the transport of biomass burning smoke is found to be
52 sporadic in nature. This sporadicity results in highly variable indicators of aerosol load and type
53 (Angstrom exponent and fine mode fraction) with moderately significant increases in both.
54 Regional dust and local pollution are the background aerosol in this highland region, whose
55 elevation places it close to the free troposphere. Transported smoke particles were generally
56 found to be more optical absorbing than in the lowlands: the hypothesis to explain this is the
57 significantly higher amount of water vapor in Amazonia relative to the high mountain areas. The
58 air-mass transport to La Paz was investigated using the HYSPLIT air-concentration five-days

59 back trajectories. Two different patterns were clearly differentiated: westerly winds from the
60 Pacific that clean the atmosphere and easterly winds favoring the transport of particles from
61 Amazonia.

62

63 **1.- Introduction**

64 High mountain areas are very sensitive to climate change as they host many glaciers and
65 are also involved in many cloud formation processes (e.g. Wonsick et al., 2014; Lüthi et al.,
66 2015). Particularly, high mountains in tropical areas are the host of glaciers and snow at such
67 latitudes, irrigating many rivers and thus are essential for the water supply of local population.
68 Changes in glacial and snow covers are indicators of climate change (e.g. Xu et al., 2016). The
69 Andes in South America is the largest mountain chain in the world covering a latitude range
70 from -55° S to 5° N and with many peaks above 5000 m a.s.l. The Andes mountain chain is part
71 of many countries and is a natural barrier between the bulk of the South American mainland and
72 the Pacific Ocean. It also represents a fundamental constraint on the eastern meteorology given
73 the predominance of easterly trade winds from the Atlantic Ocean. These trade winds create the
74 conditions for the South American Low Level Jet (SALLJ) that runs parallel to the mountains
75 (Ulke et al., 2011). The SALLJ exhibits an annual cycle that peaks during austral summer and is
76 the major air-mass transport mechanism in South America. Despite its low altitude (around 1500
77 m a.s.l.), it enhances moisture availability for convection in the Andes Mountains (Nogués-
78 Paegle and Mo, 1997). In other regions containing large mountain chains such as the Himalaya in
79 Asia or the Alps in Europe many studies have been done concerning trace gases (e.g.
80 Schwikowski et al., 1999; Maione et al., 2011), aerosols (e.g. Gautman et al., 2011; Zieger et al.,

81 2012) and cloud formation (e.g. Bonasoni et al., 2010). In the Andes, however, due to the lack of
82 appropriate measurements, these topics have not been studied well.

83 The Amazon Basin is a major source of anthropogenic-driven biomass-burning emissions
84 (e.g. Mishra et al., 2015), accounting for approximately 15% of total global biomass-burning
85 emissions (van der Werf et al., 2010). Depending on the vegetation burned, fires inject reactive
86 gases, greenhouse gases (e.g. as carbon dioxide (CO₂) and methane (CH₄)) and particles into
87 the atmosphere (Andreae and Merlet, 2001; Bowman et al., 2009; Remy et al., 2014). Biomass-
88 burning emissions are also a major source of organic (14-77 Tg/yr) and black carbon particles
89 (1.8-11 Tg/yr) (e.g. Bond et al., 2013). Aerosol smoke particles that are the result of biomass-
90 burning directly affect the Earth-Atmosphere radiative budget by scattering and absorbing solar
91 radiation (e.g. Jacobson, 2014) and also indirectly by acting as cloud condensation nuclei (CCN)
92 and ice nuclei (IC) and thereby changing the distribution and properties of clouds (e.g. Koren et
93 al., 2008). Biomass-burning can be the cause of serious public health issues such as extreme
94 particulate matter (PM) concentrations caused by fires in the island of Borneo and Sumatra (Eck
95 et al., 2016). Smoke from wildfires has also been associated with both increased mortality (Vedal
96 and Dutton, 2006) and morbidity (Bowman and Johnston, 2005), and may cause ~250,000
97 (73,000–435,000) premature mortalities/yr, with >90% being associated with PM (Jacobson,
98 2014).

99 In Amazonia the smoke emissions caused by agricultural burning of residues (e.g. Uriarte
100 et al., 2009) and by deforestation along the borders of Amazon forests, known as the arc of
101 deforestation (e.g. Morton et al., 2008; van Marle et al., 2016). The burned areas are commonly
102 found in Brazil, Peru, Colombia, Bolivia, Paraguay and northern Argentina. Atmospheric
103 transport patterns lead to spatial distributions of smoke that can be very different from the

104 distribution of the actual fire sources (e.g. Freitas et al., 2005). This, in turn, has differing
105 impacts on different environments and populations. As an example, many studies have been
106 carried out over Brazilian areas, including modeling transport efforts (e.g. Matichuk et al., 2008;
107 Longo et al., 2010) and the impact of smoke over both rural areas and highly populated cities
108 (e.g. Reid et al., 1998,1999; Kotchenruther et al., 1998). Also, intensive field campaigns such as
109 GOAMAZON (<http://campaign.arm.gov/goamazon2014/>) have been staged to advance the
110 understanding of absorption and aging properties of smoke, of greenhouse gases and of smoke
111 transport patterns. However, due to the enormous areas burned and the population differences as
112 well as different agricultural traditions and agricultural development between Brazil and its
113 neighbors, the study of biomass burning in the rest of South America needs to be the focus of
114 more investigations.

115 The main objective of this work is to analyze the smoke particle patterns in the Bolivian
116 Andes and surrounding areas. To that end, we focus on the long-term ground-based
117 measurements of the AERONET network acquired at the high mountain site in the city of La Paz
118 (3340 m a.s.l) and at nearby lowland sites in Brazil and Bolivia. We used the HYSPLIT model
119 (Stein et al., 2015) to interpret the origin of the air masses influencing the study region. Biomass-
120 burning smoke studies using AERONET data have been successfully carried out in Brazil (e.g.
121 Schafer et al., 2008), Africa (e.g. Eck et al., 2003, 2013; Queface et al., 2011) and in Alaska (e.g.
122 Eck et al., 2009) as well as for cases of long-range transport of biomass burning smoke in North
123 America (e.g. Colarco et al., 2003; Veselovskii et al., 2015), Europe (e.g. Alados-Arboledas et
124 al., 2011) and Asia (e.g. Noh et al., 2009). AERONET data on biomass-burning smoke have also
125 been used to improve and validate satellite retrievals (e.g. Sayer et al., 2014).

126 This work is structured as follows: Section II describes the experimental region and
127 methodology. The results are in Section III and concluding remarks in section IV.

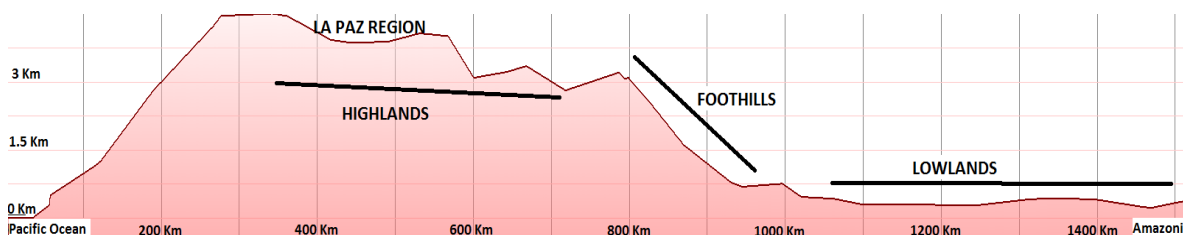
128 **2.- Experimental Region and Methodology**

129 The South American study zone of interest is in the tropical region within 10-20° South
130 and 50-70° West. The area includes three different geophysical regions: The Amazon (lowlands)
131 is characterized by tropical conditions, the high mountain regions by mountains above 6000 m
132 a.s.l. that also include flat areas known as the 'Altiplano' (highlands ~ 4000 m a.s.l.) and by a
133 transition between the two (foothills). Figure 1 shows a map of the area, including the
134 AERONET stations whose data were used in this study and an example of an elevation profile
135 from the Pacific Ocean to Amazonia crossing the La Paz region. The wet season occurs during
136 the period from December to March, and the dry season is particularly intense in the period from
137 June to September. The most important geo-atmospheric factor is the strong altitude gradient
138 between the lowlands and highlands, with its attendant large differences in water vapor content
139 and relative humidity. The city of La Paz, Bolivia (16.36° South, 68.06° West, 3439 m a.s.l.),
140 which is located in a valley surrounded by mountains of up to 5500 m a.s.l is an important focus
141 of this study. The metropolitan area includes the Andean Altiplano with a total population of
142 around 1.7 million inhabitants. The lowlands to the north and east include the stations of Rio
143 Branco, Brazil (9.95° South, 67.87° West, 212 m a.s.l.), Cuiaba, Brazil (15.50° South, 56.00°
144 West, 250 m a.s.l.) and Ji-Parana, Brazil (10.85° South, 61.80° West, 100 m a.s.l.) These stations
145 are close to small-medium sized cities with populations in the range of 120,000-600,000
146 inhabitants. The station in the Bolivian city of Santa Cruz de la Sierra (17.08° South, 63.17°
147 West, 442 m a.s.l.) with a total population of 2 million was also included in our study.

148 Anthropogenic aerosol emissions from these cities, particularly road traffic emissions, are the
149 main sources of local anthropogenic aerosol over the study region.



150



151

152 **Figure 1:** Study region including the AERONET stations used. Horizontal line in the map represents the region of
153 the elevation profile.

154 Column-integrated characterization of atmospheric aerosol was examined using
155 AERONET sun-photometry measurements. The standard AERONET instrument is the well-
156 known CIMEL CE-318-4 sun photometer. This device measures direct sun signals at 340, 380,

157 440, 500, 675, 870, and 1020 nm which are transformed into aerosol optical depths (AODs).
158 Details of AERONET sun photometers including calibration, error analysis and aerosol optical
159 properties retrievals are in Holben et al., (1998), Eck et al.,(1999) and in Smirnov et al., (2000).
160 All the data used in this study are cloud-screened and quality assured (Level 2.0).

161 Within the solar spectrum, the Angström exponent is a good indicator of the predominant
162 size of atmospheric particles (i.e. Dubovik et al., 2002): $\alpha > 1.5$ implies the predominance of
163 fine mode (submicron) aerosols while $\alpha < 0.5$ implies the predominance of coarse mode
164 (supermicron) aerosols. However, for a more accurate characterization of the relative influence
165 of fine and coarse mode particles an interpretation based solely on very high or very low values
166 of α is not straightforward. We accordingly used the Spectral Deconvolution Algorithm (SDA)
167 product incorporated into AERONET standardized processing (O'Neill et al., 2001a,b; 2003), to
168 study fine mode AOD (AOD_{fine}), coarse mode AOD (AOD_{coarse}), and fine mode fraction
169 ($\eta = AOD_{\text{fine}} / AOD$) at a reference wavelength of 500 nm.

170 In terms of aerosol microphysical properties, the operational AERONET algorithm
171 (Dubovik and King, 2000; Dubovik et al., 2000) uses sky radiances and direct sun measurements
172 as inputs and provides retrieved aerosol size distribution as well as intensive properties such as
173 aerosol refractive index, single scattering albedo (SSA) and asymmetry factor (g) (across four
174 spectral bands at 440, 675, 870, 1020 nm). However, the AERONET algorithm has specific and
175 often difficult to satisfy sky condition requirements (Holben et al., 2006) in that skies must be
176 completely clear and large scattering angles (typically larger than 50°). These limitations imply
177 that refractive index retrievals are only reliable for $AOD > 0.4$, although not for the retrieval of
178 size distribution (Holben et al., 2006). It accordingly provides low temporal resolution results
179 (generally a maximum of approximately 8 inversions per day are possible). Nevertheless,

180 retrievals that uses sky radiance measurements are the only that are able to provide retrieved
181 values of aerosol refractive index, single scattering albedo and phase function with appropriate
182 accuracy (Dubovik et al., 2006).

183 To complement AERONET retrieved aerosol microphysical properties, we compute
184 additional retrievals using the Linear Estimation technique (Veselovskii et al., 2012, 2013), that
185 uses AERONET spectral AODs measurements as input to yield high frequency estimates of
186 aerosol microphysical parameters during the whole day. The parameters retrieved using the LE
187 technique are the effective radius (r_{eff}) and the volume concentration (V). The other retrievals we
188 ran were based on the method proposed by O'Neill et al., (2005, 2008a), which, itself, is based
189 on the spectral curvature of the fine mode Angstrom slope and its spectral derivative, derived
190 from the SDA. This algorithm is used to estimate the fine mode effective radius (r_{fine}).

191 The inversions by LE are constrained in the maximum radius allowed in the inversion due
192 to the range of AODs used in the inversion (380 - 1020 nm), being improved the retrieval
193 accuracy. Measurements of $\alpha(440-870)$ are used for the selection of the maximum radius in the
194 inversion, being of 2 μm for fine mode predominance and of 10 μm for the rest of cases. Also,
195 simulations revealed that LE retrievals have an accuracy below 20% for $r_{\text{fine}} > 0.12 \mu\text{m}$, while the
196 accuracy degrades for lower r_{fine} due to the lack of sensitivity of the inversion range to these tiny
197 particles. Posterior comparisons versus AERONET retrievals showed differences of up to 10 %
198 for fine mode predominance and 20 % for coarse mode predominance. The largest uncertainties
199 were found for mixtures of both modes with differences up to 30%. Because the use of LE
200 retrievals is for supporting AERONET inversions, corrections functions are applied which
201 reduced the differences between the two retrieval schemes to generally less than 10%. We
202 remark here that AERONET uncertainties are similar to these ranges being (Dubovik et al.,

203 2000). More details about the use of Linear Estimation retrievals are in Perez-Ramirez et al.,
204 (2015). On the other hand, for the retrievals of r_{fine} using O'Neill et al., (2005, 2008a)
205 methodology, comparisons versus AERONET retrievals for the limited data set of O'Neill et al.,
206 2005 and confirmed by more recently unpublished AERONET-wide comparisons show average
207 differences $\sim 10\%$ for η values $> \sim 0.5$.

208 The HYSPLIT model (Stein et al., 2015), developed by the NOAA Air Resources
209 Laboratory, and accessible on-line at <http://www.ready.noaa.gov/HYSPLIT.php> is used to
210 compute air parcel backward-trajectories and from them assess dispersion of aerosols. The
211 meteorological data used to run the model were from 6-hourly GDAS (Global Data Assimilation
212 <http://www.emc.ncep.noaa.gov/gmb/gdas/>) output at 1° degree horizontal resolution. The total
213 trajectory time was set to 120 hours.

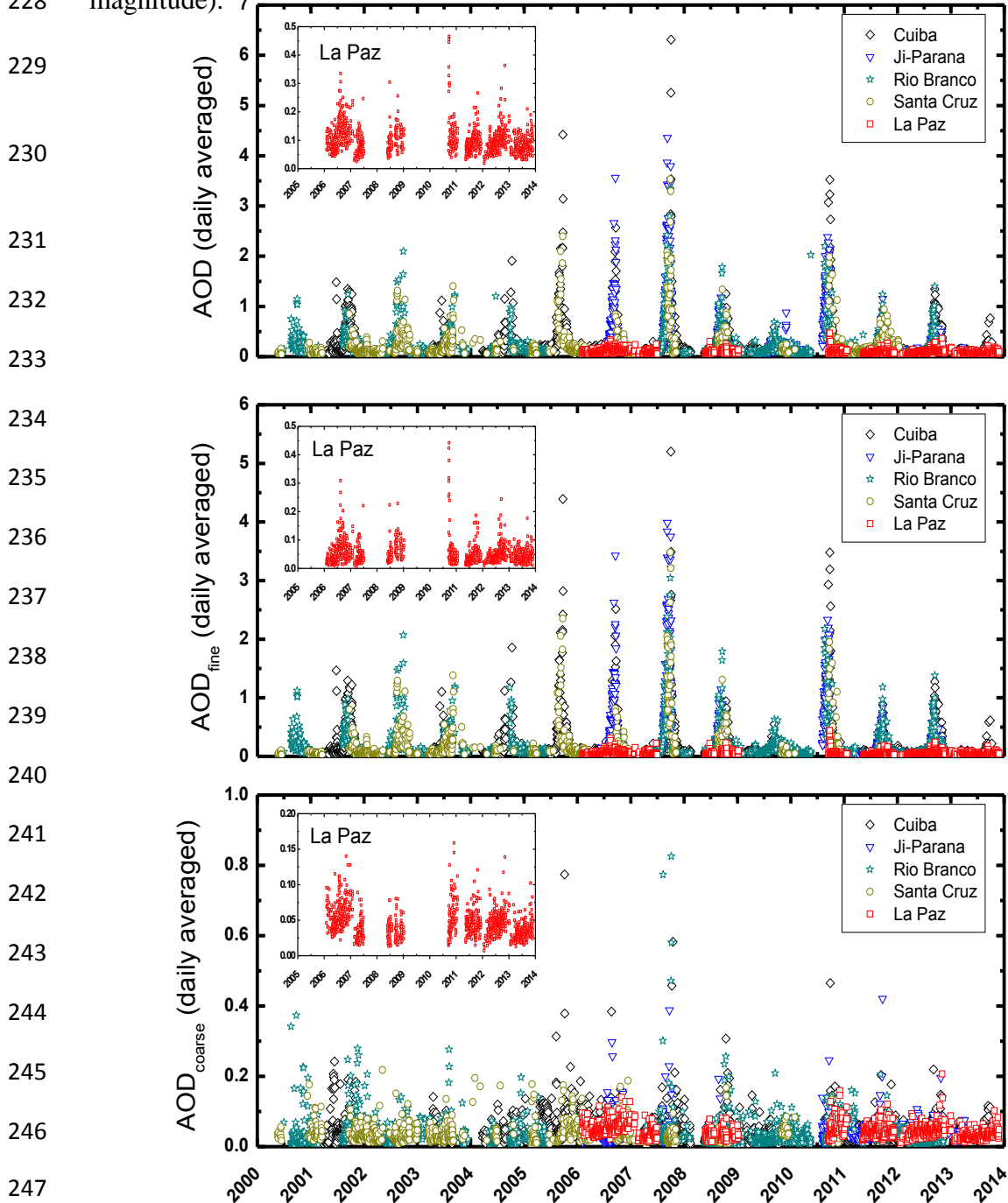
214 **3.- Results**

215 **3.1. Aerosol Optical Properties**

216 Figure 2 shows the temporal evolution of daily means of AOD, AOD_{fine} and $\text{AOD}_{\text{coarse}}$ for
217 the AERONET stations, whose data were employed in our study (with a zoomed insert of the
218 temporal plot of the highlands station of La Paz). The reference wavelength is 500 nm. Table 1
219 presents a statistical summary of the parameters in Figure 2, particularly mean values, standard
220 deviations (*STD*), medians, maxima and minima.

221 Maxima of AOD, AOD_{fine} and $\text{AOD}_{\text{coarse}}$ occur during the biomass-burning season from
222 August to October. The intensity of the biomass-burning season varies from year to year as
223 evidenced, for example, by the different maximum values of Figure 2. These intense biomass-
224 burning seasons have also been reported in the literature based on satellite observations (e.g.

225 Torres et al., 2010). During the biomass-burning season, increases in AOD_{fine} and AOD_{coarse} are
 226 observed when compared with other seasons. But the increase of AOD_{fine} is very large compared
 227 to that of AOD_{coarse} , indicating a large predominance of fine particles (by about an order of
 228 magnitude).



248 **Figure 2:** Temporal evolution of daily averaged AOD, including these of the fine and coarse mode. Reference
 249 wavelength is 500 nm.

		AOD	Alpha	AOD _{fine}	AOD _{coarse}	Eta	AOD	Alpha	AOD _{fine}	AOD _{coarse}	Eta
		Biomass-Burning Season					No Biomass-Burning Season				
Cuiaba	Mean	0.55	1.56	0.48	0.06	0.82	0.13	1.15	0.08	0.04	0.64
	STD	0.61	0.30	0.55	0.06	0.14	0.09	0.32	0.08	0.03	0.14
	Median	0.35	1.63	0.29	0.05	0.85	0.11	1.15	0.07	0.04	0.64
	Max.	6.31	2.12	5.20	0.77	0.99	0.21	2.15	0.19	0.24	0.99
	Min.	0.07	1.41	0.03	0.00	0.24	0.03	0.95	0.01	0.00	0.54
Ji Parana	Mean	0.89	1.71	0.80	0.05	0.89	0.13	1.15	0.06	0.04	0.58
	STD	0.79	0.25	0.79	0.05	0.12	0.09	0.29	0.04	0.02	0.11
	Median	0.50	1.75	0.50	0.04	0.93	0.11	1.14	0.05	0.04	0.57
	Max.	4.36	2.15	3.99	0.42	0.99	0.24	1.97	0.20	0.16	0.89
	Min.	0.07	1.55	0.04	0.01	0.54	0.03	0.95	0.01	0.01	0.20
Rio Branco	Mean	0.52	1.67	0.47	0.04	0.89	0.11	0.84	0.09	0.04	0.72
	STD	0.46	0.29	0.45	0.07	0.12	0.08	0.31	0.06	0.03	0.15
	Median	0.36	1.74	0.31	0.02	0.93	0.09	0.82	0.08	0.02	0.75
	Max.	3.53	2.40	3.22	0.92	0.99	0.19	1.92	0.15	0.18	0.98
	Min.	0.06	1.54	0.04	0.01	0.22	0.02	0.62	0.02	0.00	0.20
Santa Cruz	Mean	0.52	1.64	0.53	0.04	0.87	0.13	1.31	0.09	0.05	0.64
	STD	0.53	0.25	0.57	0.03	0.12	0.09	0.37	0.09	0.02	0.16
	Median	0.33	1.69	0.29	0.03	0.92	0.11	1.36	0.06	0.03	0.64
	Max.	3.53	2.15	3.48	0.17	0.99	0.24	2.4	0.20	0.21	0.98
	Min.	0.06	1.49	0.05	0.00	0.18	0.03	1.05	0.01	0.01	0.17
La Paz	Mean	0.12	0.95	0.07	0.05	0.55	0.09	0.84	0.04	0.04	0.48
	STD	0.06	0.30	0.06	0.02	0.15	0.04	0.31	0.03	0.02	0.13
	Median	0.11	0.95	0.05	0.05	0.53	0.08	0.82	0.04	0.04	0.48
	Max.	0.46	1.69	0.44	0.13	0.95	0.16	1.92	0.14	0.08	0.89
	Min.	0.03	0.74	0.01	0.01	0.17	0.02	0.62	0.01	0.01	0.17

250

251 **Table 1:** Mean, standard deviation (STD), median and maximum (Max.) and minimum (Min.) values of aerosol
252 optical depth (AOD), Angstrom parameter (α) between 440 and 870 nm, fine (AOD_{fine}) and coarse(AOD_{coarse}) mode
253 aerosol optical depths and relative contribution of fine mode to total optical depth (η). Data are presented for
254 biomass and non biomass-burning seasons for the stations in the lowlands (Cuiaba, Ji Parana, Rio Branco and Santa
255 Cruz) and in the highlands (La Paz). Reference wavelength for AOD, AOD_{fine}, AOD_{coarse} and η is 500 nm.

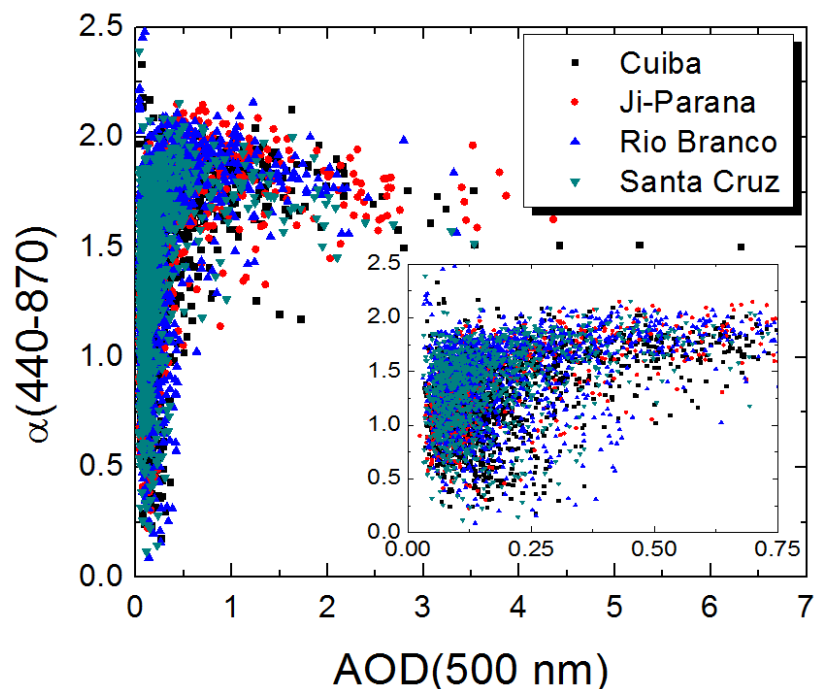
256 The differences in the maximum values of AODs among the different biomass-burning
257 seasons imply a multi-year variability in fire emissions, which is consistent with the large
258 standard deviation of AODs reported in Table 1. Emissions of smoke particles from biomass
259 burning are mostly associated with human activities. Examples of this are fires that are used for
260 forest clearing by small farmers and plantation owners who clear understory shrubbery and cut

261 forest trees. The area is burned a few months after the clearing, and, although the fires are
262 intended to only burn in limited areas, they sometimes spread beyond the targeted agricultural
263 zone and consume pristine rainforest (e.g. Torres et al., 2010). The extent and intensity of the
264 burned areas can vary from year to year.

265 To show that the data used are predominately cloud-free, Figure 3 shows $\alpha(440-870)$
266 versus AOD(500) for lowland stations. Cloud-affected data typically present $\alpha(440-870) < 0.5$
267 (O'Neill et al., 2003). In particular, AODs > 2 are associated with $\alpha(440-870)$ values that are
268 generally > 1.2 , a value which suggests minimal cloud contamination in the measurements.
269 Moreover, the number of photocounts is large enough to guarantee the quality of the
270 measurements: for very high AODs the number of photocounts registered by the AERONET
271 instruments ranged from about 50 to 20 counts for 500 nm AODs of 4 and 6 respectively at the
272 Cuiaba site, while the minimum count required for good AOD measurement is 10 (Sinyuk et al.,
273 2012).

274 The analyses of η is useful for detecting when AOD measurements are affected by thin
275 and stable cirrus clouds (O'Neill et al., 2003). Measurements affected by cirrus clouds present
276 low η because these clouds are formed by big ice crystals. Indeed, for aerosol with fine mode
277 predominance and not affected by cirrus η present high values. This approach can be applied for
278 smoke particles. The analyses performed of η values for Figure 3 data reveal that measurements
279 with AOD > 2.0 (71 days totally) present $\eta > 0.85$, suggesting no presence of clouds. For $1 <$
280 AOD < 2 were registered 220 days of measurements, and it is found that 94% with $\eta > 0.9$, and
281 only 4 days of measurements with $\eta < 0.75$ that could be associated with influence of thin cirrus
282 clouds. Finally, for 394 days of measurements that presented $0.5 < \text{AOD} < 1$, were registered
283 82% of cases with $\eta > 0.9$ and 94% with $\eta > 0.8$. The rest of the cases with lower η can be

284 associated with aerosol influenced by coarse particles, although the presence of thin cirrus clouds
285 cannot be discarded.

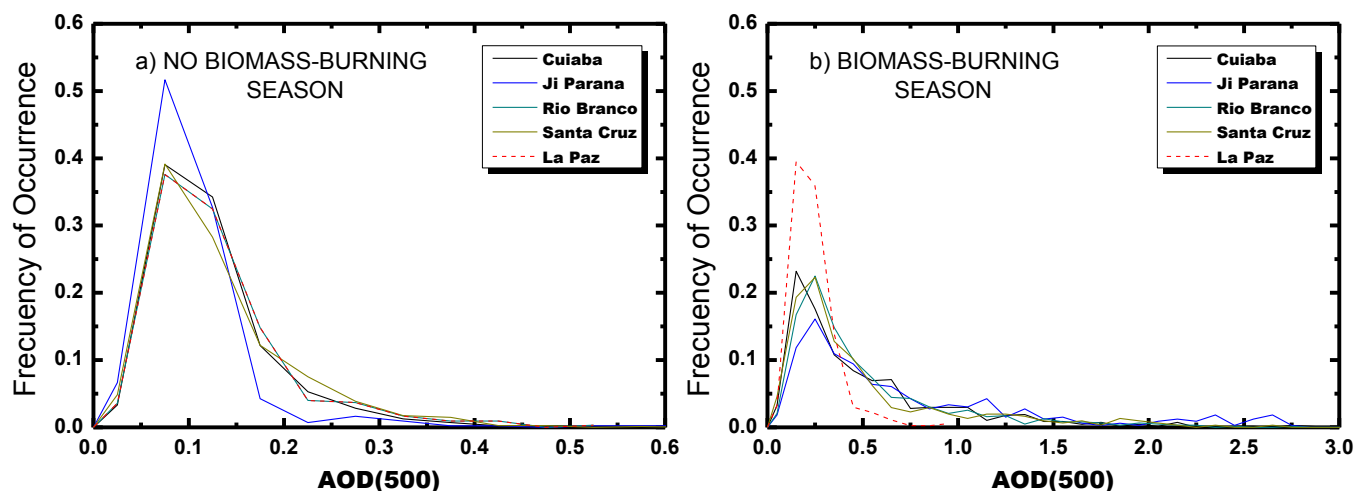


286

287 **Figure 3:** Angstrom exponent versus AOD for the measured points of Figure 2.

288 The maximum values reported in Figure 2 represent some of the largest values ever
289 registered in the AEROENT Version 2 database ([http://aeronet.gsfc.nasa.gov/cgi-](http://aeronet.gsfc.nasa.gov/cgi-bin/climo_menu_v2_new)
290 [bin/climo_menu_v2_new](http://aeronet.gsfc.nasa.gov/cgi-bin/climo_menu_v2_new)). The mean values during the biomass-burning season are also among
291 the largest monthly mean climatological values. Schafer et al., (2008) registered similar values
292 using stations located in the Amazon basin. Comparably high AOD values were also reported for
293 African biomass-burning by Eck et al., (2003, 2013). Moreover, the occurrence of very high
294 AOD values over the extended periods of time that we have reported here are only obtained in
295 very polluted parts of Asia (e.g. Eck et al., 2010), very dusty areas in the Sahara (e.g. Guirado et
296 al., 2014) and the Arabian Peninsula (e.g. Kim et al., 2011).

297 For the highland La Paz station the AOD increased during the August-October period
 298 from mean values around 0.09 to 0.12 (Table 1), but the AOD values are much lower than those
 299 in the lowlands. Although the fine mode is still predominant, the contribution of coarse mode to
 300 the total AOD cannot be ignored. The frequency histograms of AOD(500) for each station are
 301 given in Figure 4, and they show that only 7 % of data at La Paz present AOD > 0.4 while for the
 302 stations of Cuiaba, Ji Parana, Rio Branco and Santa Cruz these percentages are of 45%, 59%,
 303 44% and 41% respectively. That indicates the greater contribution of biomass-burning particles
 304 in the lowlands to the total aerosol load and to the aerosol seasonal changes.

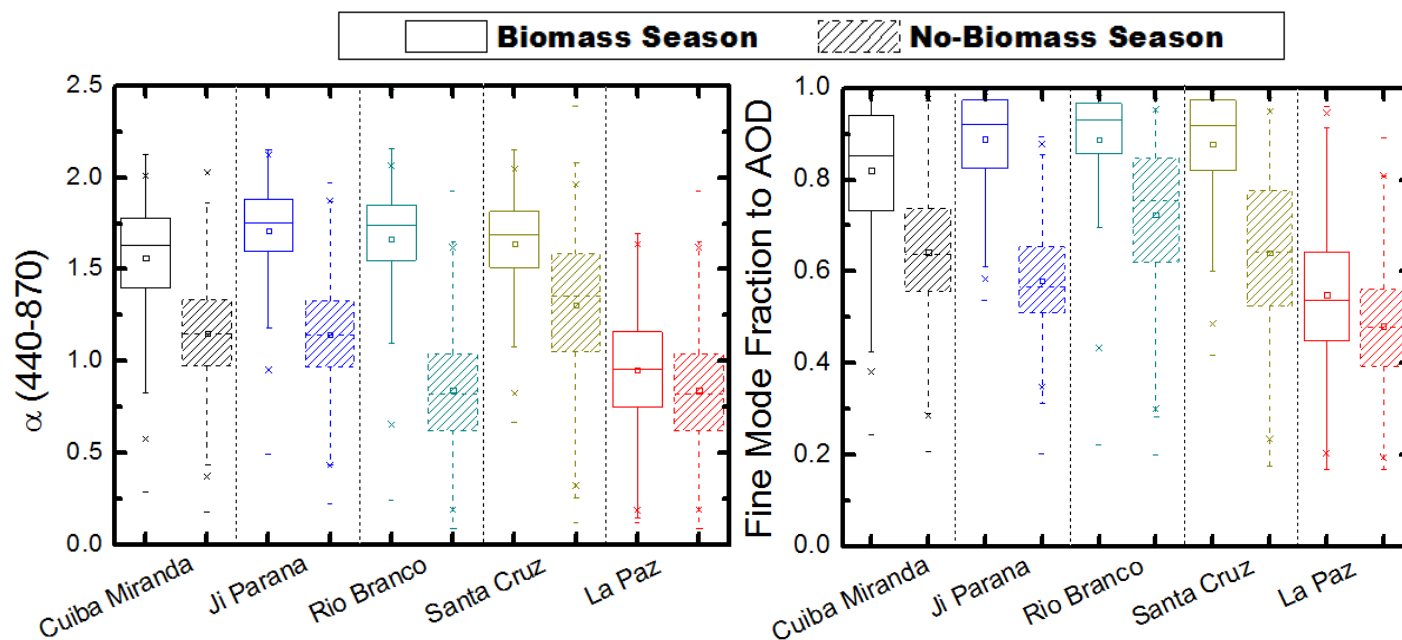


305 **Figure 4:** Frequency histograms of aerosol optical depth at 500 nm (AOD(500)) for (a) no biomass-burning and (b)
 306 biomass-burning seasons.

307 Multi-wavelength lidar measurements in the central Amazon made by Baars et al., (2012)
 308 showed that smoke plumes can reach altitudes up to 5 km. During the burning season, the
 309 reduced vegetation in the highlands implies few fires, while the large AODs in the lowlands
 310 suggests that transport of smoke particles from nearby Amazonia is the a important source of
 311 particles in the highlands. The Andes chain in the tropics is therefore a barrier for the transport of
 312 smoke to the Pacific Ocean, in agreement with the results of Bourgeois et al., (2015) using
 313 CALIPSO data.

314 Indicators of particle type predominance between biomass and non-biomass burning
 315 seasons is illustrated in Figure 5, where Box-Whisker plots of $\alpha(440-870)$ and fine mode fraction
 316 are represented. In the Box-Whisker plots, the mean is represented by a very small open square
 317 within a given rectangle. The horizontal line segment in the rectangle is the median. The top
 318 limit (top of the rectangle) represents the 75th percentile ($P75$) and the bottom limit the 25th
 319 percentile ($P25$). The lines perpendicular to the boxes are the 1st ($P1$) and 99th ($P99$) percentiles,
 320 and the crosses represent the maximum and minimum values respectively.

321



322

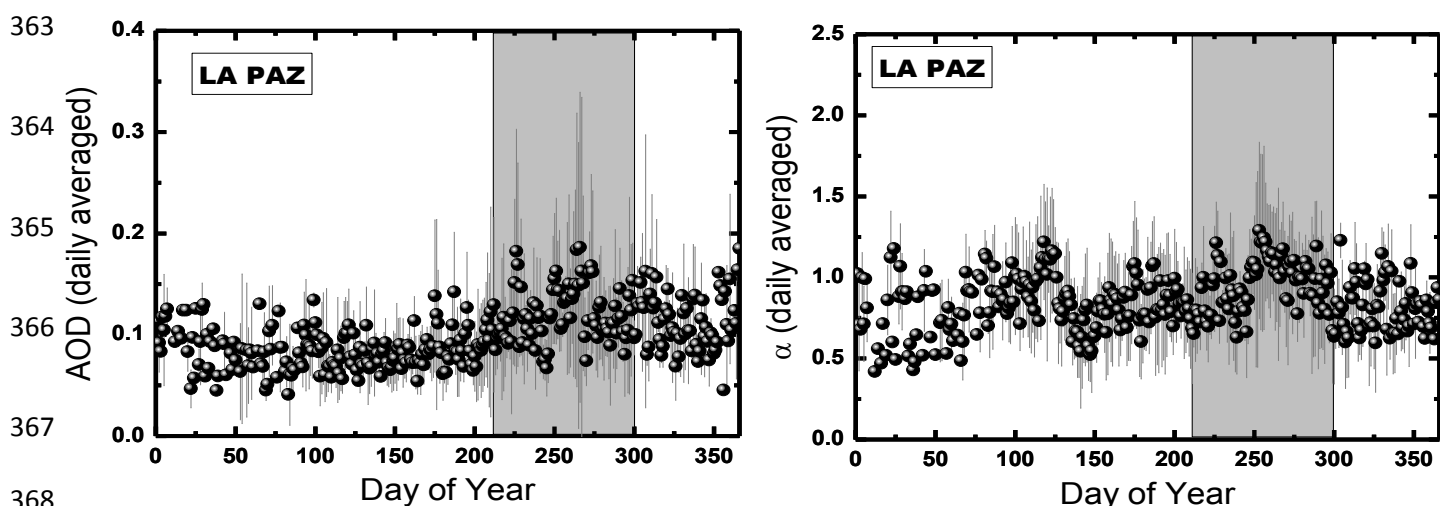
323 **Figure 5:** Box-Whisker plots during the biomass and no biomass-burning seasons of the Angstrom parameter $\alpha(440-$
 324 $870)$ and fine mode fraction to AOD for the lowlands stations (Cuiaba Miranda, Ji Parana, Rio Branco and Santa
 325 Cruz) and highlands station (La Paz). In the Box-Whisker plots, the mean is represented by a very small open square
 326 within a given rectangle. The horizontal line segment in the rectangle is the median. The top limit (top of the
 327 rectangle) represents the 75th percentile ($P75$) and the bottom limit the 25th percentile ($P25$). The lines
 328 perpendicular to the boxes are the 1st ($P1$) and 99th ($P99$) percentiles, and the crosses represent the maximum and
 329 minimum values respectively.

330

331 Figure 5 shows very high values of $\alpha(440-870)$ in the lowlands during the biomass-
332 burning seasons, with mean values of 1.5-1.7 which are similar to biomass-burning values
333 reported in the literature (e.g. Dubovik et al., 2002; Schafer et al. 2008) and, along with the
334 values of η above 0.80, indicate a predominance of fine particles. Lower values of $\alpha(440-870)$,
335 characterized by large standard deviations, are observed for the non-biomass burning seasons.
336 The mean values also vary significantly among stations (from 0.86 at Rio Branco to 1.36 at Santa
337 Cruz). These results, plus the fact that the values of η vary between 0.7 and 0.5, indicate a lack of
338 predominance of fine or coarse mode in the wet season. Indeed, a mixture of different particles
339 predominates. On the other hand, the mean Angstrom Exponent values of 0.94 and 0.85 for the
340 biomass and non-biomass burning seasons, respectively at the highland station of La Paz, are not
341 significantly different after considering the standard deviation. The same is true for η , with mean
342 values of 0.55 and 0.48 respectively. These La Paz values of $\alpha(440-870)$ and η cannot,
343 accordingly, be associated with large predominance of either fine or coarse mode.

344 The multi-year and seasonal variability of AOD and $\alpha(440-870)$ in the highland station is
345 illustrated in Figure 6 as a function of the day of the year. Mean values are represented by dots
346 and standard deviations by vertical lines. These values are the result of averaging AOD for each
347 day of the year in different years. During the biomass-burning season mean AOD at 500 nm is of
348 0.12 ± 0.06 , but the standard deviations of the means indicate AOD peaks of up to 0.35, and are
349 typical values associated with the transport of biomass-burning particles to high mountain places
350 (e.g. Perez-Ramirez et al., 2008). For other high mountain sites in the Himalayas during the pre-
351 monsoon season, values of up to 0.1 are reported at elevations of ~ 5000 m a.s.l. (Marcq et al.,
352 2010) and up to 0.5 at elevations of ~ 2000 m a.s.l. (Dumka et al., 2008). Therefore, the values
353 obtained in La Paz station are similar to high-mountain Himalayan sites affected by the transport

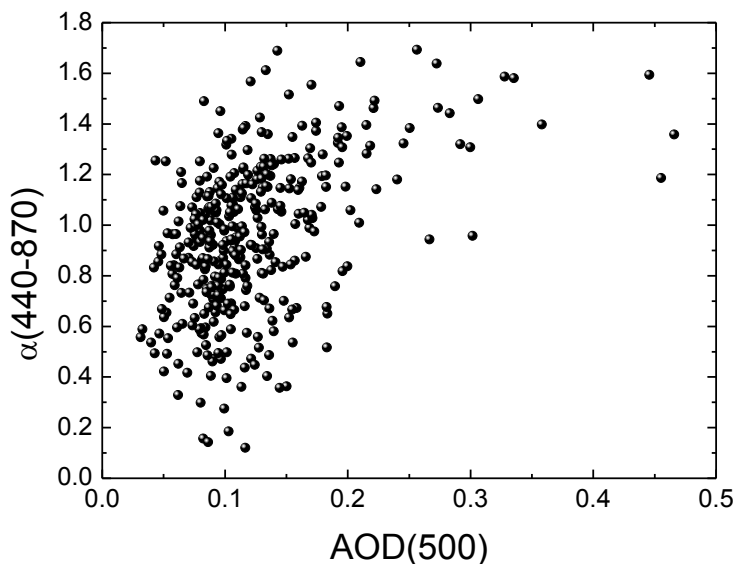
354 of pollutants. The large standard deviations of AODs in the biomass-burning season also indicate
 355 large variability, which suggests that the arrival of smoke particles occurs during sporadic events
 356 rather than as part of a continuous. AODs values during the other seasons (especially in the
 357 April-July period), are ~ 0.1 and are considered as background conditions (local
 358 origins). Therefore, biomass-burning transport to high mountains can induce AOD values of up to
 359 five times the average background conditions. In section 3.4, we study several such events in
 360 detail. The period November-March (wet season) exhibits large variability, which might be
 361 explained by meteorological factors such as wet deposition and by the less robust statistics of the
 362 smaller database associated with that period.



369 **Figure 6:** Mean AOD and Angstrom parameter ($\alpha(440-870)$), including standard deviations, for every
 370 day of the year for the highland station of La Paz. The areas shadowed in light grey represent the
 371 biomass-burning seasons.

372 The parameter $\alpha(440-870)$ shows mean values that are not significantly different during
 373 the biomass burning season as compared with the other seasons (Figure 6b). This suggests that
 374 the particle type predominance during the biomass-burning season is similar to that in other
 375 seasons (which are probably dominated by aerosols of local origin). Actually, during the
 376 biomass-burning season, mean $\alpha(440-870)$ values are around 1.0 while values for background

377 conditions (focussing on the April-July period with mean AODs of ~ 0.09) $\alpha(440-870)$ are around
378 0.85. In the wet season (November-March), the larger variability observed in Figure 6 can be
379 explained by the low AODs (< 0.05) which implies larger uncertainties in $\alpha(440-870)$.



380
381 **Figure 7:** Angstrom exponent versus AOD in the highlands station of La Paz.
382 The frequency of sporadic smoke events transported to La Paz can be observed in the
383 $\alpha(440-870)$ versus AOD graph of Figure 7 (whose dataset is limited to the biomass-burning
384 season). In order to discriminate AOD contributions associated with the transport of smoke from
385 background AODs, we established $AOD > 0.14$, which is the mean plus standard deviation value
386 during the non biomass-burning season (Table 1), as a criterion for classifying intense smoke
387 events. Analyses of Figure 7 data indicate that only 10 % of the measurements acquired during
388 the biomass-burning season exceed this threshold. The cases of smoke transport are
389 characterized by a considerably higher $\alpha(440-870)$ (1.4 ± 0.2) versus the background. Since there
390 is no other extra source than episodic biomass-burning aerosols (emissions by local sources are
391 almost constant throughout the year), the large differences in the Angstrom exponent associated

392 with smoke between lowlands (~1.8) and highlands (~1.4) suggest changes in smoke particles
393 during their transport to the highlands. This could also suggest a larger influence of local coarse
394 mode particles at La Paz since the maximum AOD values are much lower there than in the
395 Amazonian Basin.

396 **3.2. Biomass-burning and precipitation rates**

397 Table 2 reports the rainfall difference between values registered and climatological
398 values for each season. Such difference is defined here as rainfall anomaly. Data used are from
399 TRMM satellite (<http://trmm.gsfc.nasa.gov>) for the period 2002-2014 in the study area (10-20°
400 South, 50-70° West.). The mean of the TRMM data are taken as the climatological values and are
401 shown in parentheses. The ‘wet’ period was taken to be November-March, the ‘dry’ period to be
402 April-July while the biomass burning period was taken as August-October.

403 An anomalous precipitation increase during the wet period can increase the amount of
404 vegetation to be burned during the biomass-burning season (Uhl et al., 1998). Increases in
405 precipitation during the biomass-burning period favors particle wet deposition and the shortening
406 of aerosol lifetimes (Freitas et al., 2005). An increase in aerosol loads can be expected for the dry
407 and biomass burning periods due to unusually dry conditions that intensify fire activity. Such
408 links with precipitation seem to be clear for the intense biomass-burning activity (as represented
409 by AOD amplitude in Figure 2) registered in 2005-2010: positive rainfall anomalies in the wet
410 season could have increased the amount of biomass that could be burned in the following
411 burning season, while negative rainfall anomalies in the dry and / or burning seasons could have
412 favored fire activity. An exception to this pattern is 2009, which exhibits positive rainfall
413 anomalies during the dry and biomass-burning seasons and therefore lowers AODs. However, in
414 2008 a strange behavior was observed in that dry conditions were present but lower AOD values

415 were recorded compared with 2005, 2006, 2007 and 2010. The strange behavior in 2008 was also
 416 reported by Torres et al., (2010) using OMI space-borne sensor data.

	Rainfall Anomaly (mm) for different seasons			Mean AERONET AOD during Biomass-Burning Season
	Wet (199.70 mm)	Dry (42.97 mm)	Biomass-Burning (67.16 mm)	
2000	2.74	-3.64	-2.06	0.39 ± 0.29
2001	-9.46	3.56	4.74	0.47 ± 0.30
2002	-16.16	1.91	-5.02	0.49 ± 0.37
2003	-20.75	2.81	12.32	0.42 ± 0.27
2004	-2.97	-4.99	-4.35	0.44 ± 0.38
2005	12.08	-4.05	5.28	0.80 ± 0.70
2006	1.69	-9.01	0.72	0.62 ± 0.59
2007	35.70	-12.51	-6.5	1.18 ± 1.00
2008	9.20	-12.07	-1.30	0.43 ± 0.29
2009	10.02	7.27	0.17	0.20 ± 0.11
2010	3.41	-11.91	-5.91	0.95 ± 0.67
2011	5.77	-11.57	-6.70	0.32 ± 0.21
2012	-13.08	7.28	-12.94	0.40 ± 0.27
2013	41.18	9.13	15.94	0.29 ± 0.19

417 **Table 2:** Precipitation anomaly for 'wet' (November-March), 'dry' (April-July) and biomass-burning
 418 seasons (August-October). The mean climatological values are in parentheses. The anomaly is defined as
 419 the difference between registered and climatological values for each season. All precipitation data were
 420 acquired by the TRMM satellite and are the average over the area 10-20 South and 50-70 West. The
 421 AOD column is the average, at 500 nm, across the biomass burning season for the lowland stations at
 422 Cuiaba, Ji Parana, Rio Branco and Santa Cruz. The "Wet" column represents data whose November to
 423 March period started in the previous year.

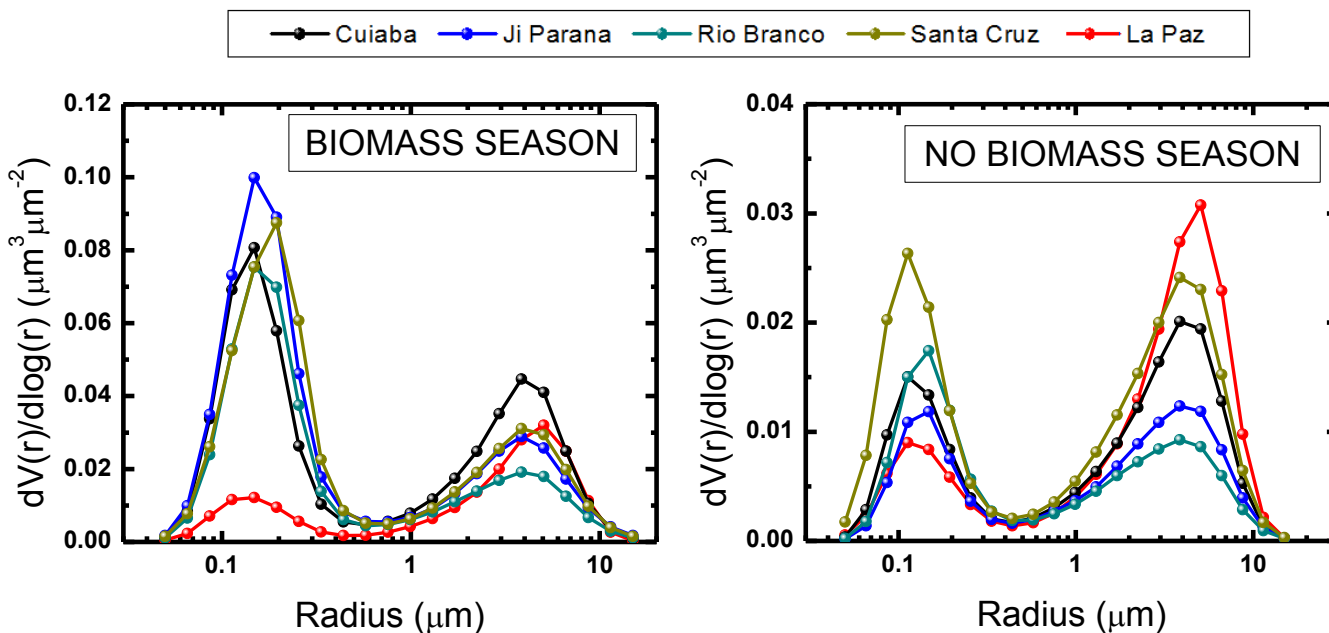
424 The 2002-2004 period (except for the dry period of 2004) exhibits an opposite pattern,
 425 with a precipitation deficit in the wet season and positive rainfall anomalies in the dry and
 426 burning seasons. The lower AODs for these years are broadly coherent with the concepts
 427 presented above on the relationship between rainfall anomaly and fire activity. However, after
 428 2011 the type of reasoning that we have employed above to make the link between rainfall
 429 anomaly and fire activity is not followed, as a continuous reduction of AODs and fire activity
 430 has been observed independently of precipitation. Specific regulations and/or economic forces as

431 suggested by Koren et al., (2007, 2009) could have helped to reduce fire activity. More years of
432 data and perhaps different level of correlation analyses have to be investigated.

433 **3.2. Aerosol Particle Sizes**

434 Figure 8 shows the mean particle volume size distributions from AERONET almucantar
435 retrievals for the study stations, separated into biomass and non-biomass burning seasons.
436 Different scales are used in the Y-axes between both seasons to better visualize size distribution
437 shapes. This figure indicates that during the biomass-burning season the fine mode largely
438 predominates for the lowland stations. Very similar size distributions for biomass-burning have
439 been reported in the literature (e.g. Eck et al., 2003; Schafer et al., 2008). However, in the
440 highlands the size distribution exhibits two modes with approximately the same volumetric
441 relevance, although that does not imply that both modes have the same optical effect (in the
442 visible spectral range, for the same volume, AOD_{fine} is larger than AOD_{coarse}). This is broadly
443 consistent with the previous results of the $\alpha(440-870)$ and η analysis: the coarse mode could be
444 associated with the injection of dust particles from the Andean Altiplano, either by traffic re-
445 suspension or regional winds: On-going studies with in-situ instrumentation are revealing that 50
446 % of PM₁₀ particles are associated with mineral dust (Alastuey et al., 2017). Fine mode particles
447 are likely associated with anthropogenic activity (e.g. vehicle emissions) and with the transport
448 of smoke particles. On the other hand, during the non-biomass burning season, the maxima of
449 volume size distributions are lower in accordance with the lower AODs. It is also observed for
450 all the stations that no mode predominates, but rather, there is an apparent mixture of different
451 types of particles. This result is also consistent with the intermediate values of $\alpha(440-870)$ and η
452 noted above. For La Paz, the two modes are explained by the same mechanism noted for the

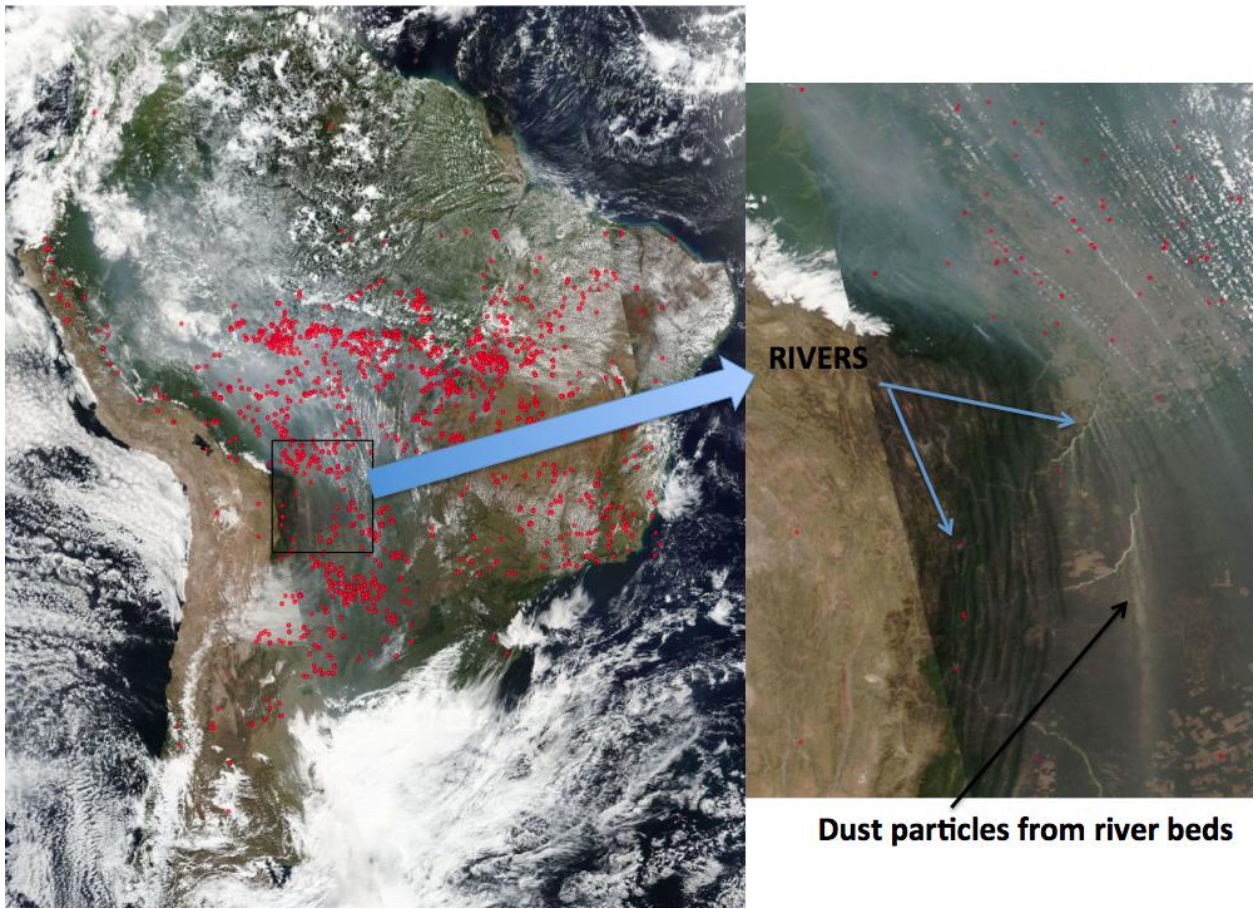
453 biomass-burning case, although the fine mode volume is smaller due to the absence of
 454 transported smoke particles.



455
 456 **Figure 8:** Mean columnar volume size distributions for the lowland stations and highland (La Paz), both for biomass
 457 and no biomass-burning seasons.

458 The stations in the lowlands, Santa Cruz and Cuiaba show a relevant coarse mode, which
 459 is present in both seasons. This coarse mode can be associated with different local sources of
 460 dust. Transport of dust from river beds is a possible explanation, as is illustrated in Figure 9
 461 which shows a true color image for the lowland area on 12th September 2016. The image is
 462 composed by the different images acquired by MODIS (Aqua and Terra) and VIIRS space
 463 systems (images available at <http://go.nasa.gov/2eULwP1>). The low level jet which runs parallel to
 464 the mountain with southerly direction is observed from the clouds and smoke transport patterns.
 465 Making a zoom on the river areas, transported dust plumes are observed. Injections of dust from
 466 riverbeds have been also observed in Alaska (Crusius et al., 2011). In South America, other
 467 regions that could be responsible for transport of dust to the lowlands is the Chaco plain that

468 spreads to the Andes foothills through Bolivia, Argentina and Paraguay, and include some of the
469 largest tributary rivers and delta rivers in the world (Latrubesse et al., 2012). From more southern
470 locations, injections of salt particles in the atmosphere have been observed from the Mar
471 Chiquita Lake (Bucher and Stein, 2016). The Andean region has other possible sources of dust
472 particles such as the Salar de Uyuni or the Atacama Desert (Gaiero et al., 2013). The high
473 latitudes of these two places could have more influence on the injection of particles in the
474 lowlands. Nevertheless, more analysis is needed to study the impact and properties of dust
475 particles in the tropical region of South America.



476
477 **Figure 9:** True color image of South America from the composition of images from MODIS (Aqua and Terra) and
478 VIIRS space-systems for 12th September 2016. A zoom is made on the lowlands in Bolivia.
479

480 Measurements of water vapor mixing ratio, w , derived from different meteorological
481 stations in Bolivia are available for more than 10 years, both for the lowlands and the highlands.
482 For the wet period (November-March) when most precipitation occurs, the highest values of
483 were found (around 19 g/Kg and 8 g/Kg for the lowlands and highlands, respectively). For the
484 dry period (April-July) with very little precipitation the lowest values are found (around 14 g/Kg
485 and 4 g/Kg for the lowlands and highlands, respectively). However, for the biomass-burning
486 season values are in the middle (around 16.5 g/Kg and 5.5 g/Kg for the lowlands and highlands,
487 respectively) indicating the presence of enough water vapor in the atmosphere to favor cloud
488 development which therefore, reduces the number of measurements that fulfil the completely
489 cloud-free sky AERONET criteria for retrieving aerosol microphysical properties. Therefore, due
490 to AODs measurements only require direct sun measurements, LE retrievals and O'Neill et al.,
491 (2005) methodology are used to obtain r_{eff} and r_{fine} , respectively, and complement AERONET
492 retrievals. Actually, during all of the biomass-burning seasons, the number of Level 2.0 retrievals
493 obtained using the almucantar retrieval was 738, 750, 1017, 262 and 206 for the Rio Branco, Ji
494 Parana, Cuiaba, Santa Cruz and La Paz stations, respectively. The number of higher temporal
495 resolution (spectral) retrievals using the LE technique were respectively 16189, 6343, 25017,
496 6719 and 18220 – this is a significant increase in the number of retrievals for the La Paz station
497 compared with the AERONET almucantar retrievals.

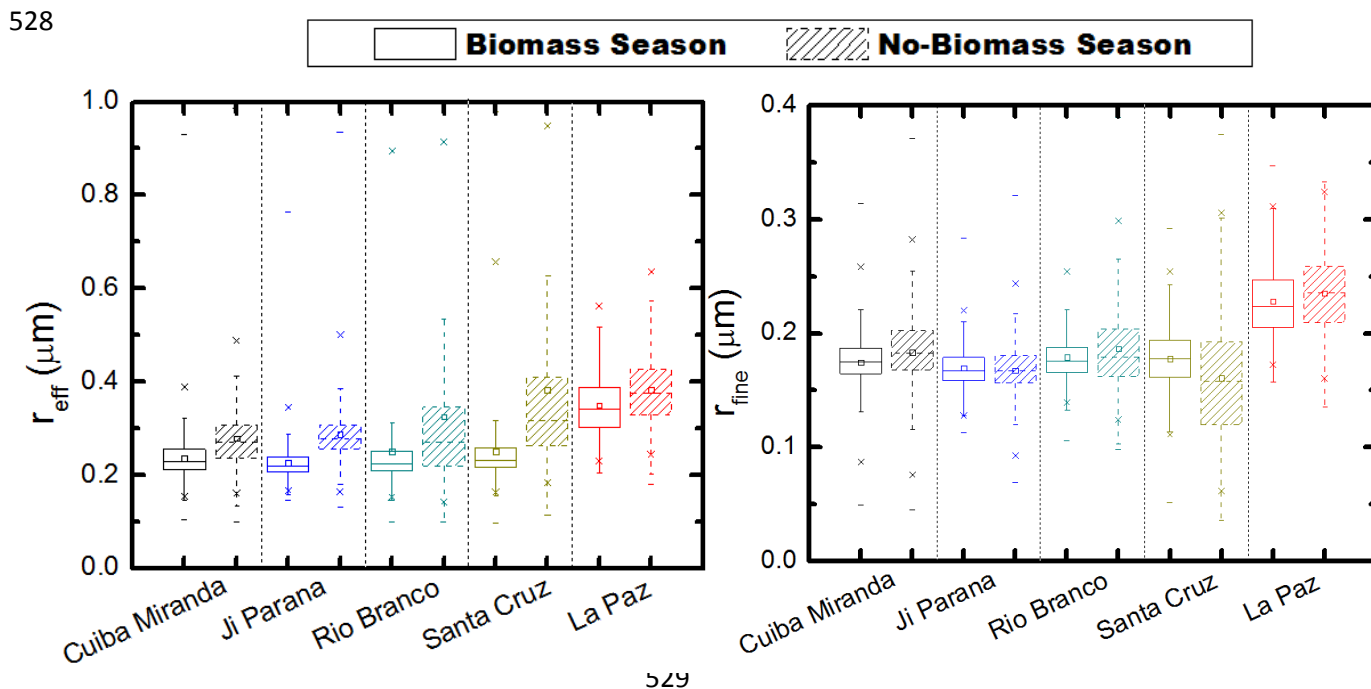
498 To understand the spatial differences in retrieved particle radii, station by station, Box-
499 Whisker plots of r_{eff} and r_{fine} , separated into biomass-burning and non biomass-burning seasons,
500 are shown in Figure 10. Table 3 summarizes the main statistical parameters of these plots. Linear
501 Estimation and O'Neill et al., (2005) retrievals are used. Similar patterns and statistics were
502 obtained using only AERONET retrieval data, although less robust statistically. During the

503 biomass-burning season the similarity of the mean values and the low standard deviations of both
504 parameters in the lowlands is remarkable: both of these comparisons indicate an approximate
505 homogeneity in the biomass-burning process with respect to particle size. The relatively large
506 variability in the non biomass-burning season can be explained by the highly variable
507 background aerosol conditions with mixtures of different aerosol types prevailing. The typically
508 larger uncertainties in r_{eff} and r_{fine} for low aerosol loads can also explain some of the increased
509 variability. The Santa Cruz station shows larger r_{eff} during the non biomass-burning season
510 which, as noted before, could be associated with coarse particles transported from local riverbeds
511 as described in association with Figure 9.

512 The highlands show systematically larger values of r_{eff} and r_{fine} independently of the
513 season. The slightly lower values of both parameters during the biomass-burning season can be
514 explained by the transport of smoke particles which, as previously noted, are predominantly fine
515 mode. Aging of the transported particles (e.g. Eck et al., 2003; O'Neill et al., 2008b) could
516 explain the larger r_{eff} and r_{fine} . The permanent coarse mode associated with dust on the Altiplano
517 could also have an influence in terms of an increase in r_{eff} . The wind regime in the high
518 mountains can favour accumulation of particles and can explain the larger values of r_{fine}
519 compared to the lowlands (Vuille, 1999).

520 The dependences of particle size on aerosol load is illustrated in Figure 11 where we
521 represent r_{eff} and r_{fine} versus the AOD at 500 nm for the combination of all lowland data. Again,
522 Linear Estimation and O'Neill et al., (2005) are used for the retrievals of r_{eff} and r_{fine} ,
523 respectively. We constrained the data plotted to conditions of $\text{AOD} > 1.0$ in order to limit the
524 study to smoke particles only. Higher temporal-resolution retrievals of r_{eff} and r_{fine} because do
525 provide larger datasets and also do allow retrievals for very high AODs which and may well be

526 favoured in the case of partly cloudy skies (see our argument above for the greater probability of
 527 clouds being associated with smoke aerosols).



530 **Figure 10:** Box-Whisker plots during the biomass and no biomass-burning seasons of the effective radius (r_{eff}) and
 531 fine mode effective radius (r_{fine}) for the lowland stations (Cuiaba Miranda, Ji Parana, Rio Branco and Santa Cruz)
 532 and the highland station (La Paz). In the Box-Whisker plots, the mean is represented by a very small open square
 533 within a given rectangle. The horizontal line segment in the rectangle is the median. The top limit (top of the
 534 rectangle) represents the 75th percentile ($P75$) and the bottom limit the 25th percentile ($P25$). The lines
 535 perpendicular to the boxes are the 1st ($P1$) and 99th ($P99$) percentiles, and the crosses represent the maximum and
 536 minimum values respectively.

537 Figure 11 shows linear trends of r_{eff} and r_{fine} with AOD increases. Similar patterns were obtained
 538 by using the operational AERONET almucantar retrieval algorithm, although the lower number
 539 of data introduced more uncertainty in the linear regressions. Actually, maximum AODs for
 540 AERONET retrievals were for ~ 3.2 , while for data of Figure 11 that maximum is for ~ 6.0 . Root-
 541 mean-square differences are ~ 0.027 for r_{eff} and ~ 0.016 for r_{fine} . The results of the linear fits
 542 shown in Figure 11 indicate that r_{fine} is nominally more sensitive to changes in AOD (the slope of
 543 the regression line is larger). The difference, for example, between the minimum and maximum
 544 AOD values of 1.0 and 6.0 is $0.035 \mu\text{m}$ for the associated r_{eff} regression line. This is small

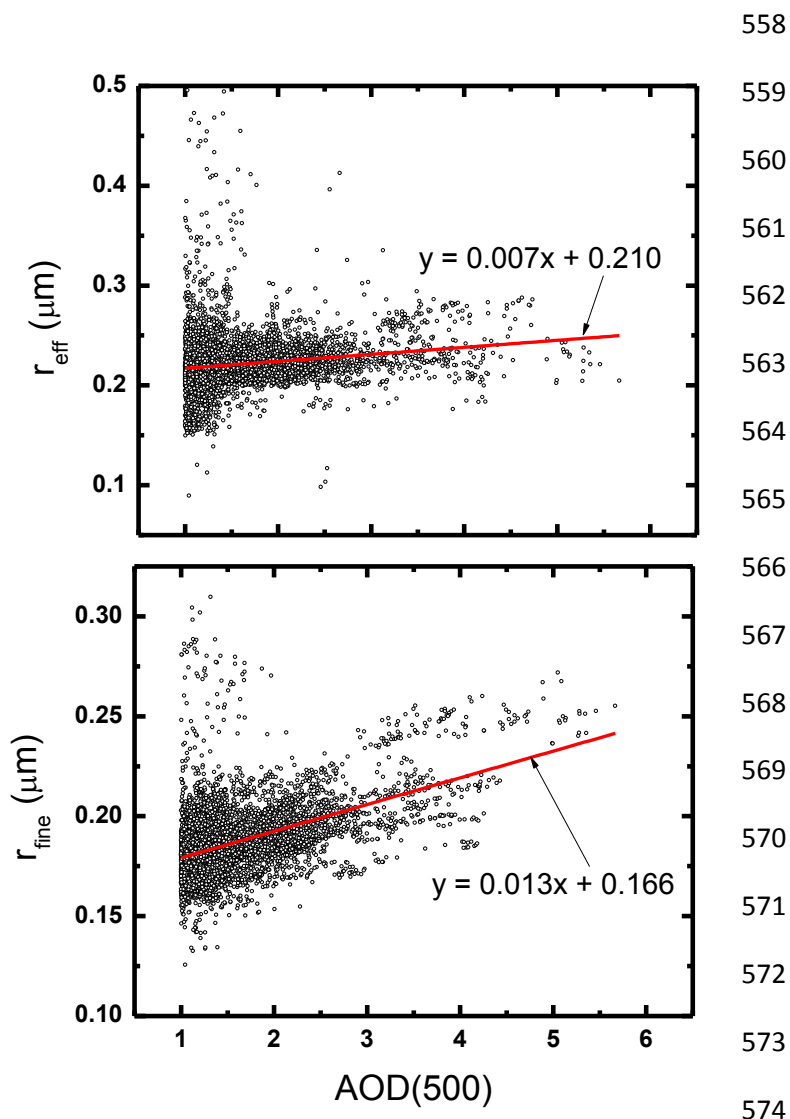
		r_{eff}	r_{fine}	r_{eff}	r_{fine}
		Biomass-Burning		No Biomass	
Cuiaba	Mean	0.24	0.18	0.27	0.20
	STD	0.05	0.03	0.07	0.04
	Median	0.23	0.18	0.27	0.20
	Max.	0.93	0.31	0.99	0.38
Ji Parana	Mean	0.22	0.17	0.29	0.16
	STD	0.03	0.02	0.06	0.05
	Median	0.22	0.17	0.28	0.17
	Max.	0.76	0.28	0.93	0.35
Rio Branco	Mean	0.25	0.18	0.32	0.19
	STD	0.11	0.02	0.18	0.03
	Median	0.22	0.17	0.27	0.18
	Max.	1.05	0.32	1.01	0.38
Santa Cruz	Mean	0.25	0.18	0.38	0.13
	STD	0.08	0.03	0.19	0.06
	Median	0.23	0.17	0.31	0.12
	Max.	0.97	0.28	1.17	0.39
La Paz	Mean	0.34	0.22	0.38	0.24
	STD	0.07	0.03	0.08	0.04
	Median	0.34	0.16	0.37	0.23
	Max.	1.14	0.35	1.08	0.51

546

547 **Table 3:** Mean, standard deviation (STD), median and maximum (Max.) values of effective radius (r_{eff}) and effective
548 radius of the fine mode (r_{fine}). Data are presented for biomass and no biomass-burning seasons for the lowland
549 stations (Cuiaba, Ji Parana, Rio Branco and Santa Cruz) and the highlands (La Paz).

550 compared with the r_{eff} values. The analogous r_{fine} calculation (a regression line increase of 0.065
551 μm for the same range of AODs), corresponds to a change of approximately 40%. Such large
552 aerosol loads favour the accumulation of particles in the atmosphere and, can therefore favor
553 particle aging. For example, larger r_{fine} and r_{eff} have been found during the night due mainly to
554 particle accumulations (e.g. Pérez-Ramírez et al., 2012). Also, coagulation rates increase as
555 particle concentration (or AOD) increases (Colarco et al., 2003). The observed trend of

556 increasing fine mode particle size in Amazonia as AOD increases is consistent with the findings
557 of Schafer et al. (2008) from AERONET almucantar retrievals.



575 **Figure 11:** Effective radius (r_{eff}) and effective radius of the fine mode (r_{fine}) versus aerosol optical depth (AOD) at
576 500 nm for the lowland data. Data selected are for AOD > 1.0.

577

578 3.3. Aerosol Single Scattering Albedo, Refractive Index and Asymmetry Factor

579 For primary (directly retrieved) optical parameters such as the refractive index and
580 derived optical parameters such as the single scattering albedo (SSA) the only source of

581 information in this study is the AERONET almucantar scan/extinction spectrum retrieval. Level
582 2.0 data, the most reliable inversion product, is constrained by several quality control criteria(see
583 Holben et al., 2006 for more details on the Level 2.0, Version 2.0 inversion criteria). Also, for
584 intensive parameters such as SSA, asymmetry factor and refractive index, the retrieval
585 uncertainties increase rapidly with decreasing AOD: this type of dependence was the motivation
586 behind the Level 2.0 criterion that limits retrievals of these parameters to conditions where
587 $AOD(440\text{ nm}) > 0.4$ (Holben et al., 2006). Because of this $AOD > 0.4$ requirement, level 2.0 La
588 Paz data over the whole database were limited to just six retrievals acquired during the 21st to
589 25th September 2010 period. Thus for this station only, we used Level 1.5 data that fulfilled the
590 Level 2.0 sky conditions - sky errors, solar zenith scattering angle criterion - while constraining
591 the retrievals to AOD values > 0.2 . The analyses are only done for the biomass-burning seasons
592 since there are little retrievals during the other seasons. The main statistical parameters of SSA,
593 real and imaginary refractive index and asymmetry factor are listed in Table 4 (for a wavelength
594 at 500 nm from linear interpolation of values at 440 and 670 nm).

595 From Table 4, SSA is generally lower in the highlands, implying more absorbing
596 particles. The imaginary part of the refractive index exhibits considerably larger values in the
597 highlands (i.e. stronger absorption with imaginary refractive index values that are, except for
598 Cuiba, greater by~ 0.005 than the lowland cases). The real part of the refractive index is
599 approximately the same for the different lowland stations, while the highland station values are
600 significantly higher. Finally, there are differences in the asymmetry factor, mostly in the near
601 infrared region, that are likely related to particle size differences. The changes between the
602 lowland and highland retrieval parameters of Table 4 suggest changes in particle composition
603 (notably the real part of the refractive index).

604
605
606
607
608
609
610
611
612
613
614
615
616
617
618

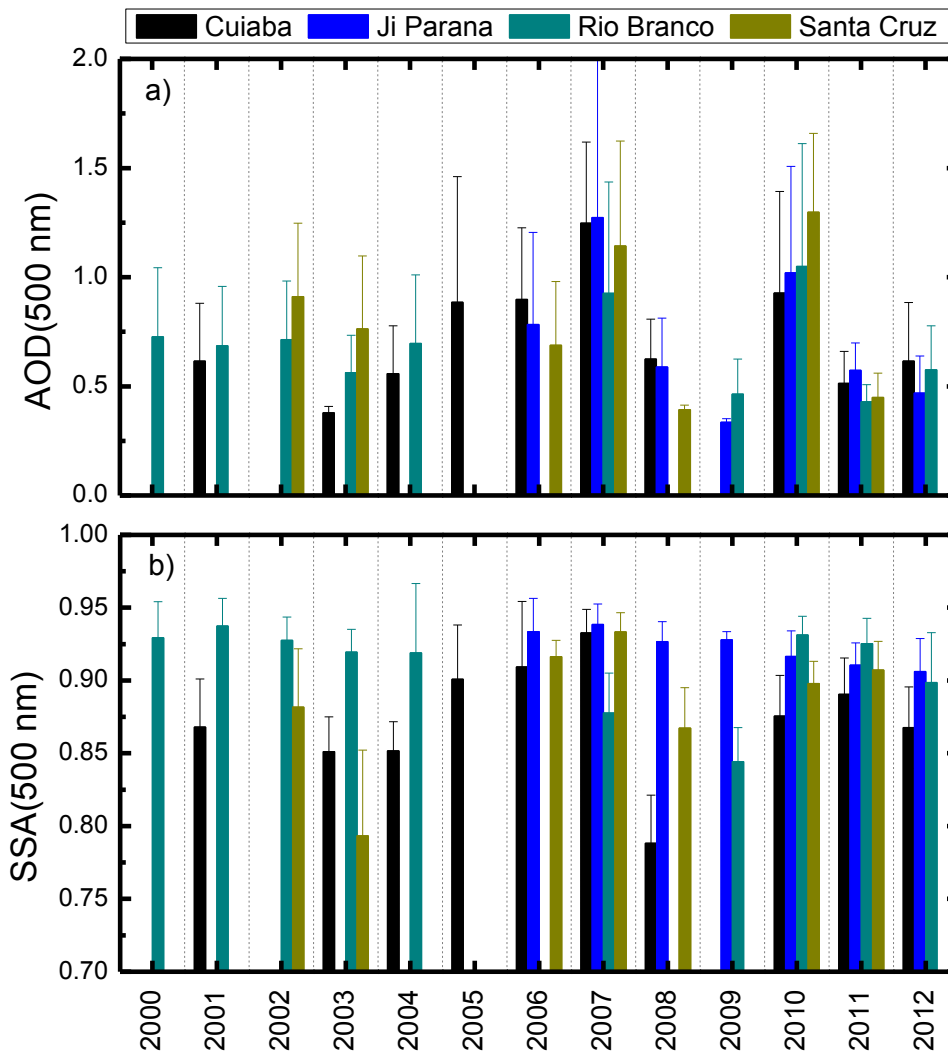
		SSA	g	m _r	m _i
Cuiaba <554>	Mean	0.88	0.65	1.46	0.019
	STD	0.05	0.02	0.06	0.010
	Median	0.88	0.65	1.47	0.017
	Max.	1.00	0.72	1.6	0.060
	Min.	0.71	0.59	1.34	0.001
Ji Parana <492>	Mean	0.92	0.65	1.48	0.011
	STD	0.02	0.02	0.05	0.004
	Median	0.93	0.65	1.48	0.011
	Max.	0.99	0.73	1.60	0.027
	Min.	0.84	0.59	1.34	0.001
Rio Branco <425>	Mean	0.91	0.66	1.47	0.015
	STD	0.04	0.02	0.05	0.007
	Median	0.92	0.73	1.47	0.013
	Max.	1.00	0.66	1.60	0.044
	Min.	0.79	0.60	1.34	0.001
Santa Cruz <158>	Mean	0.91	0.67	1.48	0.015
	STD	0.04	0.02	0.05	0.010
	Median	0.93	0.67	1.48	0.011
	Max.	0.98	0.71	1.60	0.065
	Min.	0.73	0.61	1.34	0.003
La Paz <36>	Mean	0.87	0.68	1.50	0.016
	STD	0.04	0.02	0.07	0.007
	Median	0.87	0.69	1.50	0.015
	Max.	0.93	0.72	1.60	0.036
	Min.	0.78	0.61	1.35	0.007

619 **Table 4:** Mean, standard deviation (STD), median and maximum (Max.) and minimum (Min.) values of aerosol
620 single scattering albedo (SSA), asymmetry factor (g) and real (m_r) and imaginary (m_i) part of refractive index. Data
621 are presented only for biomass-burning data as most of the data that fulfill AERONET requirements are acquired in
622 this season. These values are the result of linearly interpolating retrieval values at 440-670 to 500 nm. Data in
623 brackets represent the number of retrievals for each place.

624 Larger SSA values being associated with the long-range transport of biomass-burning
625 particles is known in the literature (e.g. Colarco et al., 2004). In the case of inter-regional
626 transport between the lowlands and the highlands, the explanation of the differences in particle
627 composition is hypothesized to be the large differences in the availability of water vapor in the
628 atmosphere commented before: hygroscopic particles grow quickly by humidification in the
629 lowlands (see, for e.g. Kotchenruther et al., 1998 and Kreidenweis et al., 2001 for general
630 discussions on humidity induced particle growth of smoke particles). The water vapor condenses

631 on the particles making them larger thereby increasing their scattering efficiency while also
632 decreasing their imaginary refractive index, resulting in making them less absorbing. At higher
633 altitudes, this particle growth effect is less probable due to the less availability of water vapor as
634 well as the fact that the water coatings of particles uplifted from the lowlands may have largely
635 evaporated. In spite of the possible mixture of smoke with local particles, the lower values of the
636 real part of refractive index in the lowlands (~ 1.47) versus the highlands (~ 1.53) would support a
637 hypothesis of humidification. It must however be borne in mind that, although humidification of
638 biomass-burning particles affects their properties in general, our retrievals involve column-
639 integrated properties, and we must accordingly be careful to not infer more from those retrievals
640 than can be justified. Indeed, these limitations indicate that more investigations into smoke
641 dynamics are needed than we carried out in our study. In particular, experimental plans would
642 need to include resources for the measurement of vertical-profiles of aerosol properties such as
643 those performed in the SAFARI-2000 field campaign (Swap et al., 2003), either by airplanes
644 (Hobbs et al., 2003) or lidar measurements (McGill et al., 2003; Veselovskii et al., 2009).

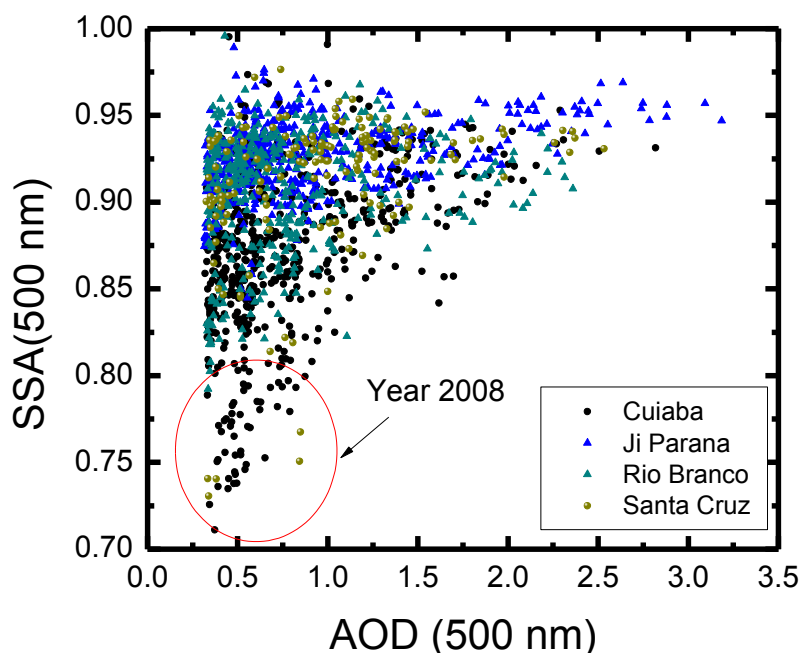
645 Because SSA is a key aerosol radiative forcing parameter, it is important to study both its
646 spatial and temporal evolution. To that end, Figure 12 shows the mean SSA and AOD means at
647 500 nm (computed from linear interpolation using 440 and 675 nm values) for the lowland
648 stations and for each biomass-burning season during the 2000-2013 period. The year to year
649 averages of Figure 12a reflect the influence of the day-to-day variations of Figure 2 with, for
650 example, peaks in 2005, 2006, 2007 and 2010 (except that the mean values of Figure 12a seem
651 larger than expected: this is because the inversion processing protocols exclude retrievals for
652 which AOD(440) is less than 0.4). With respect to the SSA, we note significant station-to-station
653 variability in Figure 12b. The SSA analysis reveals curious results: for the large AOD years



654 **Figure 12:** Temporal evolution of the means and standard deviations of (a) aerosol optical depth (AOD) and (b)
 655 single scattering albedos (SSA) during the biomass-burning seasons for the lowland. Reference wavelength is at
 656 500 nm.

657 (2005, 2006, 2007 and 2010) the values of SSA are approximately similar among the stations
 658 with an average that is close to 0.90. However, for the years of lower AODs (e.g. 2003, 2004 and
 659 2008), SSA values are lower (0.85 - 0.78) at Cuiaba and Santa Cruz, while at Rio Branco and Ji
 660 Parana the values remain around 0.92. During the years of very intense burning activity (2005,
 661 2006, 2007 and 2010) the burned area is very extensive in area: there is accordingly an enormous
 662 loading of particles in the atmosphere that arguably produce spatial homogenization of aerosol
 663 properties associated with greater regional transport dynamics. For smaller AODs the aerosols

664 are not so regionally homogenous and differences in particle properties can arise between
665 different sites. During low biomass-burning years at the southern Cuiaba and Santa Cruz sites,
666 cerrado and agricultural burning is very likely more dominant. During higher biomass-burning
667 years there would be more long-range transport of higher AOD plumes from the forest burning
668 regions towards the south and west (Freitas et al., 2005). The cerrado vegetation (savannah type)
669 burns with relatively more flaming phase combustion, thereby producing more black carbon.
670 This results in lower SSA than smoke from forest burning regions which have a higher
671 percentage of smoldering phase combustion from woody fuels therefore producing less black
672 carbon(e.g. Ward et al., 1992; Reid et al. 2005a,b).



673
674 **Figure 13:** Single scattering albedo (SSA) versus aerosol optical depth (AOD) for the complete AERONET level 2.0
675 database in the lowlands.
676 A scatterplot analysis of SSA versus AOD is shown in Figure 13. The large SSA values
677 of approximately 0.90 to 0.95 for very large AOD values are observed again for all the stations.
678 For lower AODs there are, as discussed above, site-dependences with low SSA values in Cuiaba

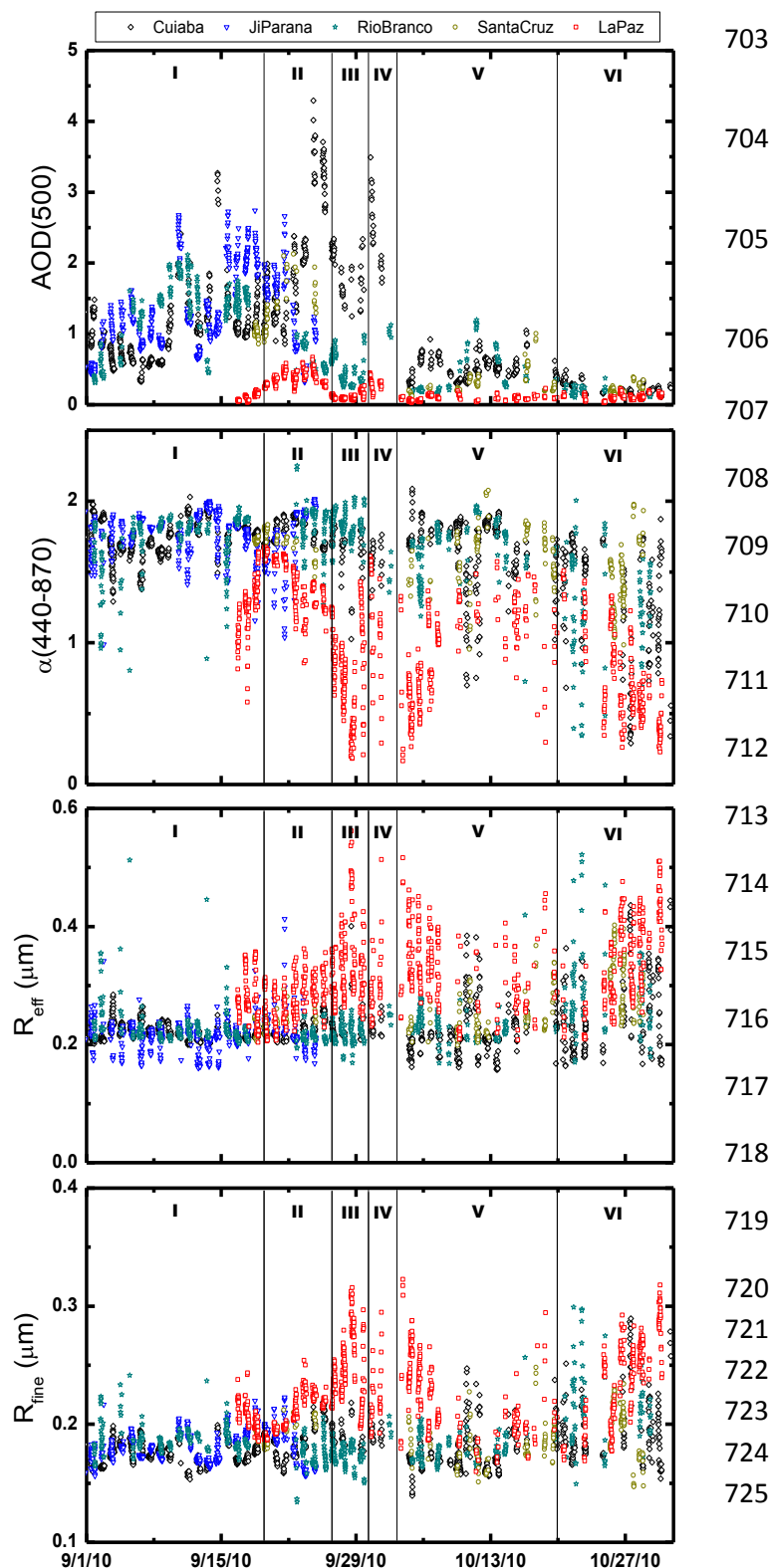
679 and Santa Cruz and larger values in Ji Parana and Rio Branco. Lower AOD with low SSA is
680 particularly observed in 2008, when an anomaly in the biomass-burning pattern was observed
681 using OMI data (Torres et al., 2010). For that year we note the rather extraordinary AERONET
682 station-to-station SSA differences (which the OMI sensor, with its coarse spatial resolution of 1°
683 $\times 1^\circ$, is largely insensitive to). The fact that the fires were less intense and sparser, and/or that
684 particle-type emission differences occurred between the savannah-like cerrado vegetation and the
685 rainforest, could explain the lack of SSA spatial homogeneity.

686 **3.4. Aerosol transport patterns to the highlands: biomass-burning case study in September-** 687 **October 2010.**

688 Our goal in this section is to illustrate the smoke patterns and transport from the lowlands
689 to the highlands during one carefully analysed biomass-burning season. We particularly
690 investigated the intense biomass-burning season of September-October 2010 when large AODs
691 (0.5) were registered at La Paz on a few days. Such AODs values are more than three times the
692 average at La Paz. Figure 14 shows the temporal evolution of AOD, $\alpha(440-870)$, r_{eff} and r_{fine} for
693 this case study at the Cuiaba, Ji-Parana, Rio Branco, Santa Cruz and La Paz stations.

694 We divided the biomass-burning case study period into five sub-periods. The first
695 subperiod (I) goes from 1 to 18 September and is characterized by strong biomass-burning in the
696 lowlands with AODs of up to 3.2. The Angstrom parameters values of around 1.8 along with $\eta >$
697 0.9 indicate a predominance of fine particles. In this period there were no measurements at the
698 La Paz station until 15th September. However, AOD values at La Paz on this day are very low
699 suggesting weak transport of biomass-particles to the Andean Altiplano. The MODIS image for
700 September 17th (Figure 15a) shows the smoke plume had pushed toward the eastern regions

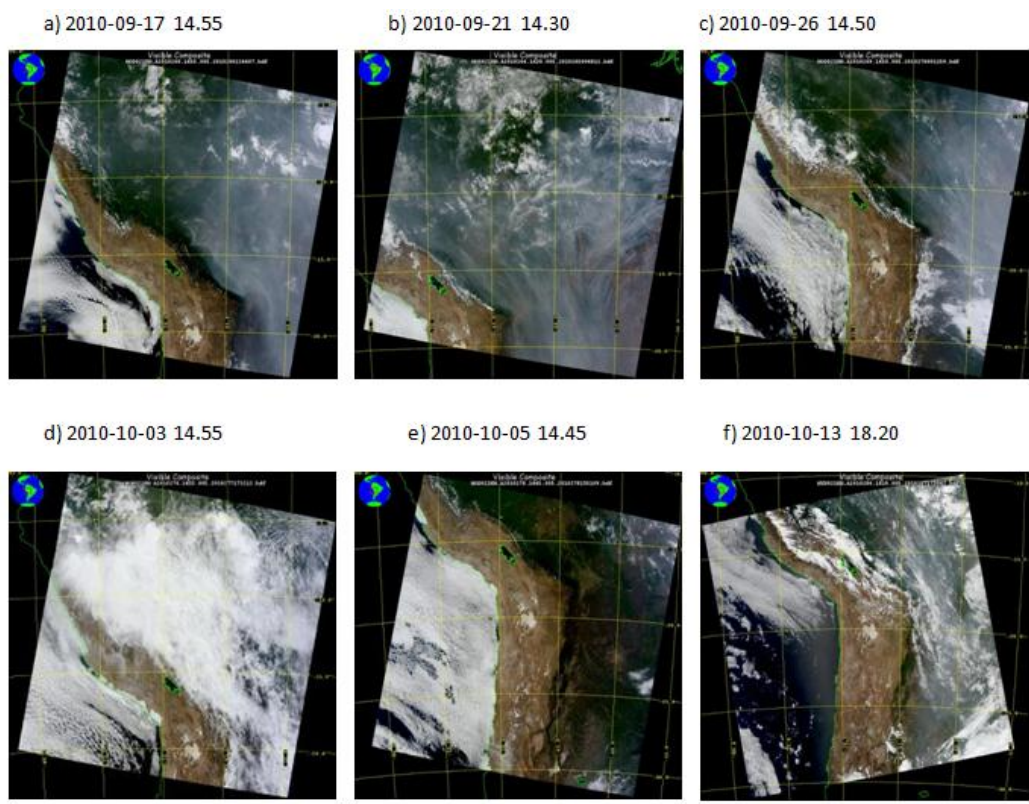
701 (Cuiaba, Ji Parana and Santa Cruz), while the areas close to Rio Branco, the foothills and the
 702 highlands, look less turbid.



703
 704
 705
 706
 707
 708
 709
 710
 711
 712
 713
 714
 715
 716
 717
 718
 719

720 **Figure 14:** Temporal evolution of
 721 aerosol optical at 500 nm (AOD),
 722 Angstrom parameter ($\alpha(440-870)$),
 723 effective radius (r_{eff}) and effective
 724 radius of the fine mode (r_{fine}) for the
 725 period August-October 2010.

726 The second subperiod (II) from 18th to 25th September includes intense biomass-burning
 727 events that reach the La Paz region. Smoke plumes can be seen to be bordering the highlands in
 728 the MODIS image for 21st September (Figure 15b). In this subperiod, the largest AODs of the
 729 entire database at La Paz were registered (up to 0.6), with a mean value of approximately 0.5. An
 730 increase in $\alpha(440-870)$ associated with the arrival of fine mode biomass-burning particles is also
 731 evident in Figure 14. The values of r_{fine} are relatively small ($\sim 0.19 \mu\text{m}$), robust and stable (low
 732 scatter during this day). After the third day (21st September), the decrease of $\alpha(440-870)$, the
 733 increase of r_{eff} and the clear increase of r_{fine} suggest fine mode aerosol aging (maybe
 734 accompanied by the presence of some coarse mode). This could be explained, for example, by
 735 the growth effects (such as coagulation) induced by the accumulation of smoke particles over
 736 several days (e.g. Reid et al., 2005a,b).

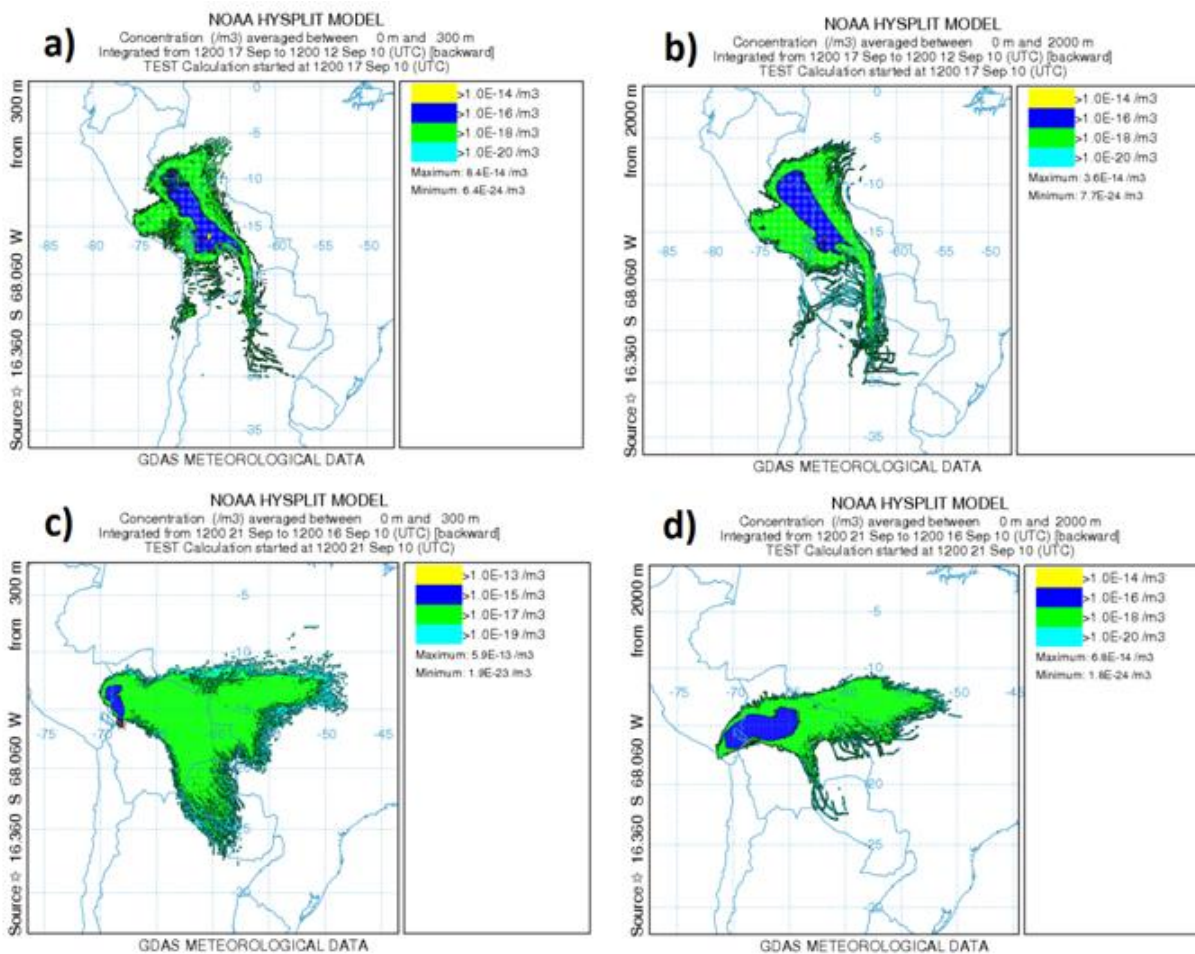


737
 738 **Figure 15:** MODIS images for (a) 17/09/2010 (b) 21/09/2010 (c)26/09/2010 (d) 03/10/2010 (e) 05/10/2010 and (f)
 739 13/10/2010

740 The study of air-mass transport to the highlands was initially done by computing
741 backward trajectories using HYSPLIT. On 17th September air-masses arriving at 1500 m a.g.l.
742 originated over the Pacific Ocean (the backward-trajectories are provided in the supplement)
743 indicate prevailing westerly winds and explain the movement of the biomass plume towards the
744 East compared to what was observed on previous days. For the intense biomass-burning on 21st
745 September, the backward-trajectories arriving at 750 and 1500 m a.g.l. (graphs in the
746 supplement) encounter the mountains producing an unrealistic calculation since the vertical
747 velocities are essentially zero. The same is observed on 17 September for the 750 m a.g.l.
748 backward-trajectory. To ameliorate this problem, HYSPLIT offers the possibility of coupling
749 backward-trajectory calculations with a Lagrangian dispersion component (Stein et al., 2015).
750 The use of air concentration backward-trajectories allows us to represent the uncertainty in the
751 calculation arising from the model's characterization of the random motions created by
752 atmospheric turbulence. The concentration pattern identifies the potential sources that might
753 have contributed to the particles arriving at the site in question. Figure 16 shows the air
754 concentration of particles at La Paz station for integration periods of 5 days (120 hours). Model
755 initialization heights were 300 and 2000 m a.g.l. (approximately in and above the planetary
756 boundary layer), with a total of 25,000 particles.

757 Figures 16a and 16b show very similar patterns of the potential sources that could have
758 influenced concentrations at the two representative heights of 300 and 2000 m a.g.l. on 17th
759 September 2010. The largest concentrations are $\sim 1\text{E-}13$ units/m³ in the area surrounding La Paz.
760 Other potential sources are located in the North and Northeast regions and in the transit area
761 between the highlands and lowlands (foothills that are locally known as 'Las Yungas'). The
762 backward air concentration evaluated every 6 hours (graphs shown in the supplement) reveal that

763 air masses that started in the previous 1-2 days had their origin in the region close to La Paz
 764 while those further from the North and the Pacific Ocean are from the last 4-5 days. Such
 765 complex patterns of air concentration are associated with the westerly winds from the Pacific at
 766 high altitudes (> 1500 m a.g.l.) and slow winds at low altitudes (< 750 m a.g.l.).



767
 768 **Figure 16:** Air concentration backward dispersion for the city of La Paz for 17/09/2010 and 21/09/2010
 769 for two altitude intervals: 0 to 300 m a.g.l. (left hand plots) and 0 to 2000 m a.g.l. (right hand plots). La
 770 Paz is identified by the tiny black empty star.

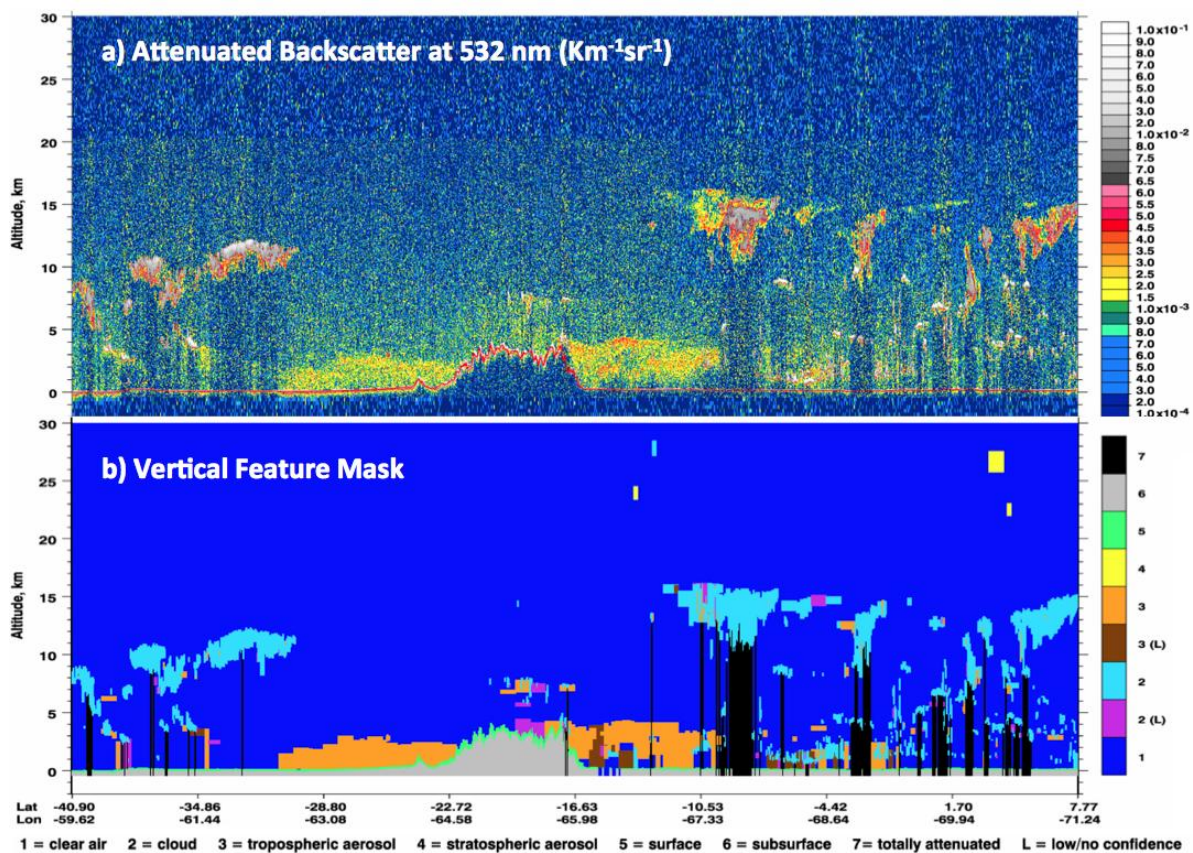
771 Figures 16c and 16d also show similar patterns for the two levels on 21th September 2010,
 772 with almost no particles transported from the west region while the largest potential sources are
 773 in the Amazonian lowlands to the east. Long-range transport is observed from the eastern regions
 774 of Bolivia and its border with Brazil, and even, for the 300 m a.g.l. level, from more distant areas

775 in Brazil, northern Paraguay and Argentina. The backward air concentration evaluations for
776 every 6 hours (graphs shown in the supplement) reveal that the areas with lower concentrations
777 correspond approximately to the previous 3-5 days while larger concentration areas correspond
778 to the previous 1-3 days.

779 Figure 17 shows CALIPSO lidar attenuated backscatter at 532 nm and vertical feature
780 mask for 20th September 2010 when the instrument passed over South America close to the study
781 region. The plot also shows the mean height above sea level. For the study region we observe
782 intense attenuated backscatter that is classified by the feature mask algorithm (Omar et al., 2009)
783 as tropospheric aerosol. According to our analyses of Figure 15 and 16 such aerosol particles
784 correspond to smoke particles. The attenuated backscatter values are close to that found in the
785 literature for smoke particles in Amazonia (e.g. Baars et al., 2012). It is clearly seen that the
786 mountains act as a natural barrier, with aerosol accumulating in the lowlands along the southern
787 and northern sides of the Andes Mountains. It is also observed that smoke plumes can reach the
788 high mountains, but with considerably lower amounts than in the lowlands. In fact, some of these
789 plumes have AOD values close to the detection limit of CALIPSO. All these findings agree with
790 our general analyses of smoke particles transported to Andean high mountains. Unfortunately,
791 CALIPSO did not cross over La Paz during the days of interest to this study and no direct
792 comparison with this station could be done.

793 The third subperiod (III) from 26th to 29th September is also characterized by air-masses
794 with origins in the Pacific Ocean (backward-trajectories not shown). Very low AODs were
795 registered again in Rio Branco and La Paz (the western locations) and the MODIS image (Figure
796 15c) shows that the smoke particles have apparently moved toward the east relative to the
797 MODIS image of Figure 15b. These findings again support the notion that strong westerly winds

798 cleaned the atmosphere. Large highland variability in $\alpha(440-870)$, r_{eff} and r_{fine} , associated with
 799 large uncertainties for low aerosol loads, is observed again. The presence of coarse mode
 800 particles at the highland station is again inferred from smaller values of $\alpha(440-870)$ and larger
 801 values of r_{eff} . The situation is however different to the East as indicated by the large AODs in
 802 Cuiaba.



803
 804 **Figure 17:** Attenuated backscatter and vertical feature mask for CALIPSO data acquired on 20th September 2010
 805 over South America. Data were acquired between 18:11:49 and 18:25:18 UTC.

806 The fourth subperiod (IV) extends from 30th September to 3rd October and is
 807 characterized by a change of the air-mass origin towards the northeast in the vicinity of Peru. For
 808 this case backward-trajectories (graphs included in the supplement) are not adversely affected by
 809 the high mountains as they were for the other dates. During this period the most relevant factor is

810 the significant amount of cloud cover (as observed in the MODIS image of Figure 15d) both in
811 the Pacific and in the Amazonia basin.

812 The last subperiods (V & VI) of Figure 14 extends from 3rd to 31st October and was
813 generally characterized by the two different air-mass patterns identified above. In this subperiod
814 we note the considerably lower aerosol load at all the stations compared to the values registered
815 in September. In general the atmosphere was clean during this subperiod as illustrated by the
816 MODIS image on the 5th of October (Figure 15e). For this day, air-masses encountered the
817 mountains and the backward dispersion air concentrations were again employed (see graphs in
818 the supplement), with patterns similar to these of Figures 16a and 16b and particles originating
819 from the northwest and southwest highlands and the Pacific Ocean. Therefore, no transport of
820 biomass-burning to La Paz was expected on October 5th, which is consistent with the weak
821 AODs of Figure 14 and the MODIS image (Figure 15e). On the other hand, between 10th and
822 15th October were registered sparse lowland biomass-burning events with some AODs above
823 0.4, high values of $\alpha(440-870)$ (close to 1.8) and stable values of r_{eff} and r_{fine} of 0.22 and 0.19
824 μm . The MODIS Aqua image for October 13th (Figure 15f) supports the characterization of
825 "sparse" and shows more intense and homogeneous biomass-burning plumes to the east of La
826 Paz. Air concentration backward-trajectory analyses were again required: the long-range
827 transport from the lowlands in the Amazon is similar to that observed for the intense smoke
828 events of the 20th September at La Paz (see graphs in the supplement). In this case, however, no
829 important AOD enhancement was registered at the La Paz station. The main reason for this is
830 likely the sparse (and probably low intensity) nature of fires in the lowlands during the 10th-15th
831 October period.

832 An analysis of wind regimes over La Paz for the August-October 2010 period reveals
833 that, at the 750 and 1500 m a.g.l. levels, 16-22% of the cases were associated with westerly
834 winds, while the rest (percentages around 80 %) were associated with easterly winds originated
835 in the lowlands at the Amazonia. Although the analyses were for the particular biomass-burning
836 season of 2010, the results may be representative of the general patterns that favour/suppress the
837 transport of smoke particles in the tropical Andean region. More in depth studies would require
838 the use of very high temporal-resolution meteorological data, and a large dataset of
839 meteorological variable measurements for a more comprehensive evaluation of these patterns.
840 Profile analyses using active remote sensing measurements are also required (e.g.
841 multiwavelength lidar) to better understand the vertical profile of the transported smoke
842 particles.

843

844 **4.- Conclusions**

845 We carried out an analysis of columnar aerosol properties in the South American tropical
846 region within 10-20° South and 50-70° West. The area includes the Amazon (lowlands), the high
847 mountain regions (highlands) and the transition between the two (foothills). Precipitation in the
848 region occurs mainly in the December-March period while the June-October period is very dry.
849 The most important geo-atmospheric factor is the strong altitude gradient between the lowlands
850 and the highlands, which implies change in vegetation and in water vapor concentration. The
851 contrast of aerosol properties between the lowlands and highlands is studied using the 2000-2014
852 AERONET measurements across the lowland stations of Rio Branco, Ji Parana, Cuiaba (stations
853 in Brazil) and Santa Cruz (Bolivia) and the highlands station of La Paz (Bolivia).

854 For the lowlands, an enhanced annual cycle in aerosol optical depth (AODs) and
855 Angstrom parameter ($\alpha(440-870)$) was observed during the biomass-burning season (August-
856 October) across all the stations. Year to year variability, with maximum AODs in 2005, 2006,
857 2007 and 2010 was observed and directly linked to biomass burning activity. Using TRMM
858 satellite data, precipitation links were studied within the context of precipitation anomalies
859 defined as the difference between annual and climatological values for the wet (November-
860 March) dry (April-July) and biomass-burning (August-October) seasons. Positive anomalies
861 during the wet season influence the amount of vegetation available to be burned, while negative
862 anomalies in the dry period favours fire activity. This hypothesis was found for the intense
863 biomass-burning seasons in 2005, 2006, 2007 and 2010, while the opposite happens in 2009 with
864 lower fire activity. After 2010, however, we did not observe such links with precipitation. Other
865 factors, such as the influence of government policies on burning practices could have had an
866 impact on our proposed relationship between rainfall anomaly and AOD and thus future
867 investigations are needed.

868 The analyses during the biomass-burning season in the lowlands showed, as expected, a
869 large predominance of fine mode particles. We also demonstrated an increase, predominantly in
870 the fine mode, of particle radius, as AOD increases. This demonstration was achieved because
871 we used the much more numerous retrievals of particle radius from spectral AOD measurements
872 in spite of the larger uncertainties compared to AERONET standard retrievals. Such a finding is
873 likely associated with the accumulation of particles. The study of the single scattering albedo
874 (SSA) also revealed interesting findings: for the years of intense biomass-burning activity, values
875 of SSA (~ 0.93) are homogeneous with very similar values among all the stations. However, for
876 the years with less intense activity, such as 2008, intra-lowland differences arise with the SSA

877 being larger (~ 0.95) at the northern stations of Rio Branco and Ji Parana and lower at the
878 southern stations of Cuiaba and Santa Cruz (SSA values with mean of ~ 0.85 and minimum
879 values even below 0.75). In the northern locations, the biomass burning of the rainforest
880 predominates while in the other locations cerrado and agricultural burning is more dominant. The
881 type of vegetation/rainforest burned could explain some of the differences observed in SSA.
882 More investigation is needed to confirm or reject this hypothesis.

883 The La Paz highlands data also showed an annual AOD cycle with maximums during the
884 biomass-burning season. These maximum values, ranging up to 0.5, are high for this region
885 where the mean AOD is approximately 0.12. Ongoing studies with in-situ instrumentation are
886 revealing the presence of anthropogenic particles during the whole year, and the only sources in
887 the Bolivian Altiplano of such particles are the local industry and road traffic in the La Paz
888 region. Also, the natural sources of highland aerosols are associated with dust from the
889 Altiplano, which is present during the whole year. Therefore, the seasonal enhancement of AOD
890 is associated with the transport of lowland smoke. However, it was found that this transport is
891 sporadic in nature. Highland particle radii showed important differences compared to lowland
892 values: For the effective radius (r_{eff}), which is sensitive to fine and coarse particles,
893 systematically larger La Paz values were likely influenced by the continuous presence of dust
894 particles from the Altiplano. The lowland station of Santa Cruz has shown the presence of coarse
895 particles which we suggested was associated with wind-driven river bed erosion. Systematically
896 larger values of fine mode radius (r_{fine}) were observed at La Paz over the whole year. Because
897 changes in r_{fine} are attributable to changes in the fine mode, these differences were thought to be
898 due to fine mode particle aging, a mechanism that is probably favoured by the high mountain
899 wind regimes. Transport of smoke particles to the highlands was associated with larger highland

900 values of particle size (both r_{fine} and r_{eff} were larger) whose growth was attributed to particle
901 aging.

902 The transported smoke particles to the highlands had lower values of SSA: large relative
903 (and specific) humidity in the lowlands favours particle growth by hygroscopicity with an
904 attendant decrease in optical absorption. In the highlands, however, relative (and specific)
905 humidity is quite low and it is likely that water, previously absorbed by the particles, evaporates.
906 The SSA retrieval numbers are, however, relatively small and it has not been possible to verify
907 this hypothesis. Comprehensive field campaigns will be needed to further identify the impact of
908 transported biomass-burning particles, preferably including simultaneous lowland and highland
909 measurements. These kinds of investigations are desired as future activities of the Global
910 Atmospheric Watch activities focussed on the station at Mount Chacaltaya(5240 m a.s.l.) in
911 Bolivia.

912 The analyses of the air-masses reaching the station of La Paz were carried out using the
913 HYSPLIT model. It has been found that the computed flow of backward-trajectories frequently
914 encounters mountains, thus introducing large uncertainties in the backward-trajectory
915 computations. Indeed, the HYSPLIT air concentration backward-dispersion has been used to
916 identify the potential sources that might have contributed to the particles arriving at the site in
917 question. The analyses of air concentration backward-dispersion have revealed that easterly
918 winds predominate allow the transport of biomass-burning particles from the Amazonian
919 lowlands, including regions of eastern Brazil, northern Paraguay and northern Argentina to the
920 highlands. On the other hand, westerly winds help to clean the atmosphere. HYSPLIT allow
921 being coupled with mesoscale models such as the Weather and Research Forecast (WRF) model,
922 and that will allow the identification of detailed transport of pollutants through the mountains.

923 Such advances are necessary for better understanding the vulnerability of the Andean high
924 mountain regions to climate change. These climate-driven studies must be combined with others
925 in glaciology to study water resources, water quality and water use efficiency, and will support
926 environmental and economic development of the nations of the Andean regions.

927 **Acknowledgments**

928 This work was supported by the Marie Skłodowska-Curie Individual Fellowships (IF)
929 ACE_GFAT (grant agreement No 659398), by the Postdoctoral Program of the University of
930 Granada (Program 8), by the NASA Atmospheric Composition Program and by the NASA
931 Aerosols, Clouds, Ecosystems mission. The work was also supported by the Andalusia Regional
932 Government through project P12-RNM-2409 by the Spanish Ministry of Economy and
933 Competitiveness and FEDER through project CGL2013-45410-R and CGL2016-81092-R , and
934 by European Union's Horizon 2020 Research and Innovation Programme under grant agreement
935 No. 654109, ACTRIS-2. The authors thankfully acknowledge the AERONET team for
936 maintaining the stations used in this work and to the NOAA Air Research Laboratory for
937 providing the HYSPLIT model.

938

939 **References**

940 Alados-Arboledas, L., Müller, D., Guerrero-Rascado, J.L., Navas-Guzmán, F., Pérez-
941 Ramírez, D., Olmo, F.J. (2011) Optical and microphysical properties of fresh biomass
942 burning aerosol retrieved by Raman lidar, and star-and sun-photometry. Geophysical
943 Research Letters 38.

944

945 Alastuey, A. (2017) Measurements of PM10 and PM2.5 at the Bolivian Andean
946 Altiplano and in La Paz region. Personal Communication, Chacaltaya GAW station Scientific
947 Steering Committee, 7 June 2017, La Paz, Bolivia.

948

949
950 Andreae, M.O., Merlet, P. (2001) Emission of trace gases and aerosols from biomass
951 burning. *Global Biogeochemical Cycles* 15, 955-966.
952

953 Baars, H., Ansmann, A., Althausen, D., Engelmann, R., Heese, B., Müller, D., Artaxo, P.,
954 Paixao, M., Pauliquevis, T., Souza, R. (2012) Aerosol profiling with lidar in the Amazon
955 Basin during the wet and dry season. *Journal of Geophysical Research: Atmospheres* 117,
956 n/a-n/a.
957

958 Bonasoni, P., Laj, P., Marinoni, A., Sprenger, M., Angelini, F., Arduini, J., Bonafè, U.,
959 Calzolari, F., Colombo, T., Decesari, S., Di Biagio, C., di Sarra, A.G., Evangelisti, F., Duchi, R.,
960 Facchini, M.C., Fuzzi, S., Gobbi, G.P., Maione, M., Panday, A., Roccatò, F., Sellegri, K., Venzac,
961 H., Verza, G.P., Villani, P., Vuillermoz, E., Cristofanelli, P. (2010) Atmospheric Brown Clouds
962 in the Himalayas: first two years of continuous observations at the Nepal Climate
963 Observatory-Pyramid (5079 m). *Atmospheric Chemistry and Physics* 10, 7515-7531.
964

965 Bond, T.C., Doherty, S.J., Fahey, D.W., Forster, P.M., Berntsen, T., DeAngelo, B.J.,
966 Flanner, M.G., Ghan, S., Kärcher, B., Koch, D., Kinne, S., Kondo, Y., Quinn, P.K., Sarofim, M.C.,
967 Schultz, M.G., Schulz, M., Venkataraman, C., Zhang, H., Zhang, S., Bellouin, N., Guttikunda,
968 S.K., Hopke, P.K., Jacobson, M.Z., Kaiser, J.W., Klimont, Z., Lohmann, U., Schwarz, J.P.,
969 Shindell, D., Storelvmo, T., Warren, S.G., Zender, C.S. (2013) Bounding the role of black
970 carbon in the climate system: A scientific assessment. *Journal of Geophysical Research:*
971 *Atmospheres* 118, 5380-5552.
972

973 Boucher, E.H., and Stein, A.F. (2016). Large salt dust storms follow a 30-year rainfall
974 cycle in the Mar Chiquita Lake (Córdoba, Argentina). *PLoS ONE*, 11(6): e0156672, doi:10.1371-
975 journal.pone.0156672.

976 Bourgeois, Q., Ekman, A.M.L., Krejci, R. (2015) Aerosol transport over the Andes
977 from the Amazon Basin to the remote Pacific Ocean: A multiyear CALIOP assessment.
978 *Journal of Geophysical Research: Atmospheres* 120, 8411-8425.
979

980 Bowman, D.M.J.S., Balch, J.K., Artaxo, P., Bond, W.J., Carlson, J.M., Cochrane, M.A.,
981 D'Antonio, C.M., DeFries, R.S., Doyle, J.C., Harrison, S.P., Johnston, F.H., Keeley, J.E.,
982 Krawchuk, M.A., Kull, A.C., Marston, J.B., Moritz, M.A., Prentice, I.C., Roos, C.I., Scott, A.C.,
983 Swetnam, T.W., van der Werf, G.R., Pyne, S.J. (2009) Fire in the Earth System. *Science* 324,
984 481-484.
985

986 Bowman, D.M.J.S., Johnston, F.H. (2005) Wildfire smoke, fire management, and
987 human health. *EcoHealth* 2, 76-80.
988

989 Colarco, P.R., Toon, O.B., Holben, B.N. (2003) Saharan dust transport to the
990 Caribbean during PRIDE: 1. Influence of dust sources and removal mechanisms on the
991 timing and magnitude of downwind aerosol optical depth events from simulations of in situ
992 and remote sensing observations. *Journal of Geophysical Research* 108, 8589.

993
994 Colarco, P.R., Schoeberl, M.R., Doddridge, B.G., Marufu, L.T., Torres, O., Welton, E.J.
995 (2004) Transport of smoke from Canadian forest fires to the surface near Washington, D.C.:
996 Injection height, entrainment, and optical properties. *Journal of Geophysical Research* 109.
997
998 Crusius, J., Schroth, A.W., Gassó, S., Moy, C.M., Levy, R.C., and Gatica, M. (2011)
999 Glacial flour dust storms in the Gulf of Alaska: Hydrologic and meteorological controls and
1000 their importance as a source of bioavailable iron. *Geophysical Research Letters*, 38, L06602
1001
1002 Dubovik, O., King, M.D. (2000) A flexible inversion algorithm for retrieval of aerosol
1003 optical properties from Sun and sky radiance measurements. *Journal of Geophysical*
1004 *Research* 105, 20673-20696.
1005
1006 Dubovik, O., Holben, B., Eck, T.F., Smirnov, A., Kaufman, Y.J., King, M.D., Tanre, D.,
1007 Slutsker, I. (2002) Variability of absorption and optical properties of key aerosol types
1008 observed in worldwide locations *Journal of the Atmospheric Sciences* 59, 590-608.
1009
1010 Dubovik, O., Sinyuk, A., Lapyonok, T., Holben, B.N., Mishchenko, M., Yang, P., Eck, T.F.,
1011 Volten, H., Muñoz, O., Veihelmann, B., van der Zande, W.J., Leon, J.-F., Sorokin, M., Slutsker, I.
1012 (2006) Application of spheroid models to account for aerosol particle nonsphericity in
1013 remote sensing of desert dust. *Journal of Geophysical Research* 111, D11208.
1014
1015 Dumka, U.C., Moorthy, K.K., Satheesh, S.K., Sagar, R., Pant, P. (2008) Short-Period
1016 Modulations in Aerosol Optical Depths over the Central Himalayas: Role of Mesoscale
1017 Processes. *Journal of Applied Meteorology and Climatology* 47, 1467-1475.
1018
1019 Eck, T.F., Holben, B.N., Reid, J.S., Dubovik, O., Smirnov, A., O'Neill, N.T., Slutsker, I.,
1020 Kinne, S. (1999) Wavelength dependence of the optical depth of biomass burning, urban,
1021 and desert dust aerosols. *Journal of Geophysical Research* 104, 31333-31349.
1022
1023 Eck, T.F., Holben, B.N., Ward, D.E., Mukelabai, M.M., Dubovik, O., Smirnov, A., Schafer,
1024 J.S., Hsu, N.C., Piketh, S.J., Queface, A., Le Roux, J., Swap, R.J., Slutsker, I. (2003) Variability of
1025 biomass burning aerosol optical characteristics in southern Africa during the SAFARI 2000
1026 dry season campaign and a comparison of single scattering albedo estimates from
1027 radiometric measurements. *Journal of Geophysical Research* 108.
1028
1029 Eck, T.F., Holben, B.N., Reid, J.S., Sinyuk, A., Hyer, E.J., O'Neill, N.T., Shaw, G.E., Vande
1030 Castle, J.R., Chapin, F.S., Dubovik, O., Smirnov, A., Vermote, E., Schafer, J.S., Giles, D., Slutsker,
1031 I., Sorokine, M., Newcomb, W.W. (2009) Optical properties of boreal region biomass
1032 burning aerosols in central Alaska and seasonal variation of aerosol optical depth at an
1033 Arctic coastal site. *Journal of Geophysical Research* 114.
1034
1035 Eck, T.F., Holben, B.N., Sinyuk, A., Pinker, R.T., Goloub, P., Chen, H., Chatenet, B., Li, Z.,
1036 Singh, R.P., Tripathi, S.N., Reid, J.S., Giles, D.M., Dubovik, O., O'Neill, N.T., Smirnov, A., Wang,
1037 P., Xia, X. (2010) Climatological aspects of the optical properties of fine/coarse mode
1038 aerosol mixtures. *Journal of Geophysical Research* 115, D19205.

1039
1040 Eck, T.F., Holben, B.N., Reid, J.S., Mukelabai, M.M., Piketh, S.J., Torres, O., Jethva, H.T.,
1041 Hyer, E.J., Ward, D.E., Dubovik, O., Sinyuk, A., Schafer, J.S., Giles, D.M., Sorokin, M., Smirnov,
1042 A., Slutsker, I. (2013) A seasonal trend of single scattering albedo in southern African
1043 biomass-burning particles: Implications for satellite products and estimates of emissions
1044 for the world's largest biomass-burning source. *Journal of Geophysical Research:*
1045 *Atmospheres* 118, 6414-6432.
1046
1047 Eck, T., Holben, B., Giles, D., Smirnov, A., Slutsker, I., Sinyuk, A., Schafer, J., Sorokin,
1048 M., Reid, J., Sayer, A., Hsu, C., Levy, R., Lyapustin, A., Wang, Y., Rahman, M.A., Liew, S.-C.,
1049 Salinas Cortijo, S.V., Li, T., Kalbermatter, D., Keong, K.L., Elifant, M., Aditya, F., Mohamad, M.,
1050 Chong, T.K., San, L.H., Choon, Y.E., Deranadyan, G., Kusumanigtyas, S., Mahmud, M. (2016)
1051 Remote sensing measurements of biomass burning aerosol optical properties during the
1052 2015 Indonesian burning season from AERONET and MODIS satellite data. In "Remote
1053 Sensing of Clouds and Aerosols: Techniques and Applications", European Geosciences
1054 Union General Assembly 2016, Vienna, Austria 17-22 April 2016. online available in
1055 <http://meetingorganizer.copernicus.org/EGU2016/EGU2016-2391-3.pdf>.
1056
1057 Freitas, S.R., Longo, K., Silva Dias, M.A.F., Silva Dias, P.L., Chatfield, R., Prins, E.,
1058 Artaxo, P., Grell, G.A., Recuero, F.S. (2005) Monitoring the transport of biomass burning
1059 emissions in South America. *Environmental Fluid Mechanics* 5, 135-167.
1060
1061 Gaiero, D.M., Simonella, L., Gassó, S., Gili, S., Stein, A.F., Sosa, P., Becchio, R., Arce,
1062 J., and Marelli, H. (2013). Ground/satellite observations and atmospheric modeling of dust
1063 storms originating in the high Puna-Altiplano deserts (South America): Implications for the
1064 interpretation of paleo-climate archives. *Journal of Geophysical Research: Atmospheres*, 118,
1065 3817-3831.
1066
1067 Gautam, R., Hsu, N.C., Tsay, S.C., Lau, K.M., Holben, B., Bell, S., Smirnov, A., Li, C.,
1068 Hansell, R., Ji, Q., Payra, S., Aryal, D., Kayastha, R., Kim, K.M. (2011) Accumulation of aerosols
1069 over the Indo-Gangetic plains and southern slopes of the Himalayas: distribution,
1070 properties and radiative effects during the 2009 pre-monsoon season. *Atmospheric
1071 Chemistry and Physics* 11, 12841-12863.
1072
1073 Guirado, C., Cuevas, E., Cachorro, V.E., Toledano, C., Alonso-Pérez, S., Bustos, J.J.,
1074 Basart, S., Romero, P.M., Camino, C., Mimouni, M., Zeudmi, L., Goloub, P., Baldasano, J.M., de
1075 Frutos, A.M. (2014) Aerosol characterization at the Saharan AERONET site Tamanrasset.
1076 *Atmospheric Chemistry and Physics* 14, 11753-11773.
1077
1078 Hobbs, P.V., Sinha, P., Yokelson, R.J., Christian, T.J., Blake, D.R., Gao, S., Kirchstetter,
1079 T.W., Novakov, T., Pilewskie, P. (2003) Evolution of gases and particles from a savanna fire
1080 in South Africa. *Journal of Geophysical Research* 108, 8485.
1081
1082 Holben, B.N., Eck, T.F., Slutsker, I., Tanre, D., Buis, J.P., Setzer, A., Vermote, E., Reagan,
J.A., Kaufman, Y.J., Nakajima, T., Lavenu, F., Jankowiak, I., Smirnov, A. (1998) AERONET- A

1083 federated instrument network and data archive for aerosol characterization. Remote
1084 Sensing of Environment 66, 1-16.
1085
1086 Holben, B.N., Eck, T.F., Slutsker, I., Smirnov, A., Sinyuk, A., Schafer, J., Giles, D.,
1087 Dubovik, O. (2006) Aeronet's Version 2.0 quality assurance criteria. Proceedings of SPIE
1088 6408, 64080Q.
1089
1090 Jacobson, M.Z. (2014) Effects of biomass burning on climate, accounting for heat and
1091 moisture fluxes, black and brown carbon, and cloud absorption effects. Journal of
1092 Geophysical Research: Atmospheres 119, 8980-9002.
1093
1094 Kim, D., Chin, M., Yu, H., Eck, T.F., Sinyuk, A., Smirnov, A., Holben, B.N. (2011) Dust
1095 optical properties over North Africa and Arabian Peninsula derived from the AERONET
1096 dataset. Atmospheric Chemistry and Physics 11, 10733-10741.
1097
1098 Koren, I., Remer, L.A., Longo, K.M. (2007) Reversal of trend of biomass burning in
1099 the Amazon. Geophysical Research Letters 34, L20404.
1100
1101 Koren, I., Martins, J.V., Remer, L.A., Afargan, H. (2008) Smoke invigoration versus
1102 inhibition of clouds over the Amazon. Science 321, 946-949.
1103
1104 Koren, I., Remer, L.A., Longo, K., Brown, F., Lindsey, R. (2009) Reply to comment by
1105 W. Schroeder et al. on "Reversal of trend of biomass burning in the Amazon". Geophysical
1106 Research Letters 36, L03807.
1107
1108 Kotchenruther, R.A., Hobbs, P.V. (1998) Humidification factors of aerosols from
1109 biomass burning in Brazil. Journal of Geophysical Research 103, 32081-32089.
1110
1111 Kreidenweis, S.M., Remer, L.A., Brientjes, R., Dubovik, O. (2001) Smoke aerosol from
1112 biomass burning in Mexico: Hygroscopic smoke optical model. Journal of Geophysical
1113 Research 106, 4831-4844.
1114
1115 Latrubesse, E.M., Stevaux, J.C., Cremon, E.H., May, J.-H., Tatum, S.H., Hurtado, M.A.,
1116 Bezada, M., Argollo, J.B. (2012). Late Quaternary megafans, fans and fluvio-aeolian interactions
1117 in the Bolivian Chaco, Tropical South America. Paleogeography, Paleoclimatology,
1118 Palaeoecology, 356-357, 75-88.
1119
1120 Longo, K.M., Freitas, S.R., Andreae, M.O., Setzer, A., Prins, E., Artaxo, P. (2010) The
1121 Coupled Aerosol and Tracer Transport model to the Brazilian developments on the
1122 Regional Atmospheric Modeling System (CATT-BRAMS) – Part 2: Model sensitivity to the
1123 biomass burning inventories. Atmospheric Chemistry and Physics 10, 5785-5795.
1124
1125 Lüthi, Z.L., Škerlak, B., Kim, S.W., Lauer, A., Mues, A., Rupakheti, M., Kang, S. (2015)
1126 Atmospheric brown clouds reach the Tibetan Plateau by crossing the Himalayas.
1127 Atmospheric Chemistry and Physics 15, 6007-6021.

1128 Maione, M., Giostra, U., Arduini, J., Furlani, F., Bonasoni, P., Cristofanelli, P., Laj, P.,
1129 Vuillermoz, E. (2011) Three-year observations of halocarbons at the Nepal Climate
1130 Observatory at Pyramid (NCO-P, 5079 m a.s.l.) on the Himalayan range. *Atmospheric
1131 Chemistry and Physics* 11, 3431-3441.
1132
1133 Marcq, S., Laj, P., Roger, J.C., Villani, P., Sellegri, K., Bonasoni, P., Marinoni, A.,
1134 Cristofanelli, P., Verza, G.P., Bergin, M. (2010) Aerosol optical properties and radiative
1135 forcing in the high Himalaya based on measurements at the Nepal Climate Observatory-
1136 Pyramid site (5079 m a.s.l.). *Atmospheric Chemistry and Physics* 10, 5859-5872.
1137
1138 Matichuk, R.I., Colarco, P.R., Smith, J.A., Toon, O.B. (2008) Modeling the transport and
1139 optical properties of smoke plumes from South American biomass burning. *Journal of
1140 Geophysical Research* 113.
1141
1142 McGill, M.J., Hlavka, D.L., Hart, W.D., Welton, E.J., Campbell, J.R. (2003) Airborne lidar
1143 measurements of aerosol optical properties during SAFARI-2000. *Journal of Geophysical
1144 Research* 108, 8493.
1145
1146 Mishra, A.K., Lehahn, Y., Rudich, Y., Koren, I. (2015) Co-variability of smoke and fire
1147 in the Amazon basin. *Atmospheric Environment* 109, 97-104
1148
1149 Morton, D.C., Defries, R.S., Randerson, J.T., Giglio, L., Schroeder, W., Van Der Werf,
1150 G.R. (2008) Agricultural intensification increases deforestation fire activity in Amazonia.
1151 *Global Change Biology* 14, 2262-2275.
1152
1153 Nogues-Paegle, J., Mo, K. (1997) Alternating wet and dry conditions over South
1154 America during summer. *Monthly Weather Review* 125.
1155
1156 Noh, Y.M., Müller, D., Shin, D.H., Lee, H., Jung, J.S., Lee, K.H., Cribb, M., Li, Z., Kim, Y.J.
1157 (2009) Optical and microphysical properties of severe haze and smoke aerosol measured
1158 by integrated remote sensing techniques in Gwangju, Korea. *Atmospheric Environment* 43,
1159 879-888.
1160
1161 Omar, A. H., Winker, D. M., Kittaka, C., Vaughan, M. A., Liu, Z., Hu, Y., and Hostetler, C.
1162 A.. (2009) The CALIPSO automated aerosol classification and lidar ratio selection algorithm,
1163 *Journal of Atmospheric and Oceanic Techniques*, 26, 1994–2014, 2009.
1164
1165 O'Neill, N.T., Dubovik, O., Eck, T.F. (2001a) Applied Optics. Modified Ångström
1166 exponent for the characterization of submicrometer aerosols 40, 2368-2375.
1167
1168 O'Neill, N.T., Eck, T.F., Holben, B.N., Smirnov, A., Dubovik, O., Royer, A. (2001b)
1169 Bimodal size distribution influences on the variation of Ångström derivatives in spectral
1170 optical depth space. *Journal of Geophysical Research* 106.
1171
1172 O'Neill, N.T., Eck, T.F., Smirnov, A., Holben, B.N., Thulasiraman, S. (2003) Spectral
1173 discrimination of coarse and fine mode optical depth. *Journal of Geophysical Research* 108.

1174
1175 O'Neill, N.T., Thulasiraman, S., Eck, T.F., Reid, J.S. (2005) Robust optical features of
1176 fine mode size distributions: Application to the Québec smoke event of 2002. *Journal of*
1177 *Geophysical Research* 110, D011207.
1178
1179 O' Neill, N.T., Thulasiraman, S., Eck, T.F., Reid, J.S. (2008a) Correction to "Robust
1180 optical features of fine mode size distributions: Application to the Québec smoke event of
1181 2002". *Journal of Geophysical Research* 113, D24203.
1182
1183 O'Neill, N.T., Pancrati, O., Baibakov, K., Eloranta, E., Batchelor, R.L., Freemantle, J.,
1184 McArthur, L.J.B., Strong, K., Lindenmaier, R. (2008b) Occurrence of weak, sub-micron,
1185 tropospheric aerosol events at high Arctic latitudes. *Geophysical Research Letters* 35.
1186
1187 Pérez-Ramírez, D., Aceituno, J., Ruiz, B., Olmo, F., Alados-Arboledas, L. (2008)
1188 Development and calibration of a star photometer to measure the aerosol optical depth:
1189 Smoke observations at a high mountain site. *Atmospheric Environment* 42, 2733-2738.
1190
1191 Pérez-Ramírez, D., Lyamani, H., Olmo, F.J., Whiteman, D.N., Alados-Arboledas, L.
1192 (2012) Columnar aerosol properties from sun-and-star photometry: statistical
1193 comparisons and day-to-night dynamic. *Atmospheric Chemistry and Physics*, 12, 9719-
1194 9738.
1195
1196 Pérez-Ramírez, D., Veselovskii, I., Whiteman, D.N., Suvorina, A., Korenskiy, M.,
1197 Kolgotin, A., Holben, B., Dubovik, O., Siniuk, A., Alados-Arboledas, L. (2015) High temporal
1198 resolution estimates of columnar aerosol microphysical parameters from spectrum of
1199 aerosol optical depth by linear estimation: application to long-term AERONET and star-
1200 photometry measurements. *Atmospheric Measurement Techniques* 8, 3117-3133.
1201
1202 Queface, A.J., Piketh, S.J., Eck, T.F., Tsay, S.-C., Mavume, A.F. (2011) Climatology of
1203 aerosol optical properties in Southern Africa. *Atmospheric Environment* 45, 2910-2921.
1204
1205 Reid, J.S., Hobbs, P.V., Ferek, R.J., Blake, D.R., Martins, J.V., Dunlap, M.R., Liousse, C.
1206 (1998) Physical, chemical, and optical properties of regional hazes dominated by smoke in
1207 Brazil. *Journal of Geophysical Research* 103.
1208

1209 Reid, J.S., Eck, T.F., Christopher, S.A., Hobbs, P.V., Holben, B.N. (1999) Use of the
1210 Angstrom exponent to estimate the variability of optical and physical properties of aging
1211 smoke particles in Brazil. *Journal of Geophysical Research* 104.
1212
1213 Reid, J.S., Eck, T.F., Christopher, S.A., Koppmann, R., Dubovik, O., Eleuterio, D.P.,
1214 Holben, B.N., Reid, E.A., Zhang, J. (2005a) A review of biomass burning emissions part III:
1215 intensive optical properties of biomass burning particles. *Atmospheric Chemistry and*
1216 *Physics* 5, 827-849.
1217

1218 Reid, J.S., Koppmann, R., Eck, T.F., Eleuterio, D.P. (2005b) A review of biomass
1219 burning emissions part II: intensive physical properties of biomass burning particles.
1220 Atmospheric Chemistry and Physics 5, 799-825.
1221

1222 Remy, S., Kaiser, J.W. (2014) Daily global fire radiative power fields estimation from
1223 one or two MODIS instruments. Atmospheric Chemistry and Physics 14, 13377-13390.
1224

1225 Sayer, A.M., Hsu, N.C., Eck, T.F., Smirnov, A., Holben, B.N. (2014) AERONET-based
1226 models of smoke-dominated aerosol near source regions and transported over oceans, and
1227 implications for satellite retrievals of aerosol optical depth. Atmospheric Chemistry and
1228 Physics 14, 11493-11523.
1229

1230 Schafer, J.S., Eck, T.F., Holben, B.N., Artaxo, P., Duarte, A.F. (2008) Characterization of
1231 the optical properties of atmospheric aerosols in Amazônia from long-term AERONET
1232 monitoring (1993–1995 and 1999–2006). Journal of Geophysical Research 113.
1233

1234 Schwikowski, M., Brütsch, S., Gäggeler, H.W., Schotterer, U. (1999) A high-resolution
1235 air chemistry record from an Alpine ice core: Fiescherhorn glacier, Swiss Alps. Journal of
1236 Geophysical Research: Atmospheres 104, 13709-13719.
1237

1238 Smirnov, A., Holben, B.N., Eck, T.F., Dubovik, O., Slutsker, I. (2000) Cloud-screening
1239 and quality control algorithms for the AERONET database. Remote Sensing of Environment
1240 73, 337-349.
1241

1242 Sinyuk, A., Holben, B.N., Smirnov, A., Eck, T.F., Slutsker, I., Schafer, J.S., Giles, D.M.,
1243 Sorokin, M. (2012) Assessment of error in aerosol optical depth measured by AERONET
1244 due to aerosol forward scattering. Geophysical Research Letters 39, L23806.
1245

1246 Stein, A.F., Draxler, R.R., Rolph, G.D., Stunder, B.J.B., Cohen, M.D., Ngan, F. (2015)
1247 NOAA's HYSPLIT Atmospheric Transport and Dispersion Modeling System. Bulletin of the
1248 American Meteorological Society 96, 2059-2077.
1249

1250 Swap, R.J., Annegarn, H.J., Suttles, J.T., King, M.D., Platnick, S., Privette, J.L., Scholes,
1251 R.J. (2003) Africa burning: A thematic analysis of the Southern African Regional Science
1252 Initiative (SAFARI 2000). Journal of Geophysical Research: Atmospheres 108, n/a-n/a.
1253

1254 Torres, O., Chen, Z., Jethva, H., Ahn, C., Freitas, S.R., Barthia, P.K. (2010) OMI and
1255 MODIS observations of the anomalous 2008-2009 Southern Hemisphere biomass burning
1256 seasons. Atmospheric Chemistry and Physics 10, 3505-3513.
1257

1258 Uhl, C., Kauffman, J.B., Cummings, D.L. (1998) Fire in Venezuelan Amazon 2:
1259 Environmental conditions necessary for forest fires in the evergreen rainforest of
1260 Venezuela. Oikos 53, 176-184.
1261

1262 Ulke, A.G., Longo, K.M., Freitas, S.R., (2011) Biomass burning in south America:
1263 transport patterns and impacts., in: Matovic, D. (Ed.), Biomass - Detection, Production and
1264 usage.
1265

1266 Uriarte, M., Yackulic, C.B., Cooper, T., Flynn, D., Cortes, M., Crk, T., Cullman, G.,
1267 McGinty, M., Sircely, J. (2009) Expansion of sugarcane production in São Paulo, Brazil:
1268 Implications for fire occurrence and respiratory health. *Agriculture, Ecosystems &*
1269 *Environment* 132, 48-56.
1270

1271 van der Werf, G.R., Randerson, J.T., Giglio, L., Collatz, G.J., Mu, M., Kasibhatla, P.S.,
1272 Morton, D.C., DeFries, R.S., Jin, Y., van Leeuwen, T.T. (2010) Global fire emissions and the
1273 contribution of deforestation, savanna, forest, agricultural, and peat fires (1997–2009).
1274 *Atmospheric Chemistry and Physics* 10, 11707-11735.
1275

1276 Van Marle, M.J.E., Field, R., van der Werf, G.R., Estrada de Wagt, I.A., Houghton, R.A.,
1277 Rizzo, L.V., Artaxo, P., and Tsigaridis, K. (2016) Fire and deforestation dynamics in
1278 Amazonia (1973-2014). *Global Biogeochemical Cycles*, 31, doi:10.1002/2016GB005445.
1279

1280 Vedal, S., Dutton, S.J. (2006) Wildfire air pollution and daily mortality in a large
1281 urban area. *Environ Res* 102, 29-35.
1282

1283 Veselovskii, I., Whiteman, D.N., Kolgotin, A., Andrews, E., and Korenskii, M. (2009)
1284 Demonstration of aerosol property profiling by multiwavelength lidar under varying
1285 relative humidity conditions. *Journal of Atmospheric and Oceanic Technology*, 26, 1543-
1286 1557.

1287 Veselovskii, I., Dubovik, O., Kolgotin, A., Korenskiy, M., Whiteman, D.N.,
1288 Allakhverdiev, K., Huseyinoglu, F. (2012) Linear estimation of particle bulk parameters
1289 from multi-wavelength lidar measurements. *Atmospheric Measurement Techniques* 5,
1290 1135-1145.
1291

1292 Veselovskii, I., Whiteman, D.N., Korenskiy, M., Kolgotin, A., Dubovik, O., Perez-
1293 Ramirez, D., Suvorina, A. (2013) Retrieval of spatio-temporal distributions of particle
1294 parameters from multiwavelength lidar measurements using the linear estimation
1295 technique and comparison with AERONET. *Atmospheric Measurement Techniques* 6, 2671-
1296 2682.
1297

1298 Veselovskii, I., Whiteman, D.N., Korenskiy, M., Suvorina, A., Kolgotin, A., Lyapustin, A.,
1299 Wang, Y., Chin, M., Bian, H., Kucsera, T.L., Pérez-Ramírez, D., Holben, B. (2015)
1300 Characterization of forest fire smoke event near Washington, DC in summer 2013 with
1301 multi-wavelength lidar. *Atmospheric Chemistry and Physics* 15, 1647-1660.
1302

1303 Vuille, M. (1999) Atmospheric circulation over the Bolivian Altiplano during dry and
1304 wet periods and extreme phases of the southern oscillation. *International Journal of*
1305 *Climatology*, 19, 1579-1600.
1306

1307 Ward, D.E., Susott, R.A., Kauffman, J.B., Babbitt, R.E., Cummings, D.L., Dias, B., Holben,
1308 B.N., Kaufman, Y.J., Rasmussen, R.A., and Setzer, W. (1992) Smoke and fire characteristics
1309 for cerrado and deforestation burns in Brazil: BASE-B Experiment. Journal of Geophysical
1310 Research, 97, 14601-14619.

1311
1312 Wonsick, M.M., Pinker, R.T., Ma, Y. (2014) Investigation of the "elevated heat pump"
1313 hypothesis of the Asian monsoon using satellite observations. Atmospheric Chemistry and
1314 Physics 14, 8749-8761.

1315

1316 Xu, Y., Ramanathan, V., Washington, W.M. (2016) Observed high-altitude warming
1317 and snow cover retreat over Tibet and the Himalayas enhanced by black carbon aerosols.
1318 Atmospheric Chemistry and Physics 16, 1303-1315.

1319

1320 Zieger, P., Kienast-Sjögren, E., Starace, M., von Bismarck, J., Bukowiecki, N.,
1321 Baltensperger, U., Wienhold, F.G., Peter, T., Ruhtz, T., Collaud Coen, M., Vuilleumier, L.,
1322 Maier, O., Emili, E., Popp, C., Weingartner, E. (2012) Spatial variation of aerosol optical
1323 properties around the high-alpine site Jungfrauoch (3580 m a.s.l.). Atmospheric Chemistry
1324 and Physics 12, 7231-7249.

1325